

2020-10-16

Metformin enhances anti-mycobacterial responses by educating CD8+ T-cell immunometabolic circuits

Julia Bohme
Singapore Immunology Network

Et al.

Let us know how access to this document benefits you.

Follow this and additional works at: <https://escholarship.umassmed.edu/oapubs>



Part of the [Bacterial Infections and Mycoses Commons](#), and the [Immunology and Infectious Disease Commons](#)

Repository Citation

Bohme J, Martinez N, Kornfeld H, Singhal A. (2020). Metformin enhances anti-mycobacterial responses by educating CD8+ T-cell immunometabolic circuits. Open Access Publications by UMMS Authors. <https://doi.org/10.1038/s41467-020-19095-z>. Retrieved from <https://escholarship.umassmed.edu/oapubs/4431>



Creative Commons License



This work is licensed under a [Creative Commons Attribution 4.0 License](#).

This material is brought to you by eScholarship@UMMS. It has been accepted for inclusion in Open Access Publications by UMMS Authors by an authorized administrator of eScholarship@UMMS. For more information, please contact Lisa.Palmer@umassmed.edu.

Metformin enhances anti-mycobacterial responses by educating CD8⁺ T-cell immunometabolic circuits

Julia Böhme¹, Nuria Martinez², Shamin Li^{1,3}, Andrea Lee¹, Mardiana Marzuki¹, Anteneh Mehari Tizazu¹, David Ackart⁴, Jessica Haugen Frenkel⁴, Alexandra Todd⁴, Ekta Lachmandas⁵, Josephine Lum¹, Foo Shihui¹, Tze Pin Ng⁶, Bennett Lee¹, Anis Larbi¹, Mihai G. Netea ^{5,7}, Randall Basaraba⁴, Reinout van Crevel⁵, Evan Newell ^{1,3}, Hardy Kornfeld ² & Amit Singhal ^{1,8,9,10} ✉

Patients with type 2 diabetes (T2D) have a lower risk of *Mycobacterium tuberculosis* infection, progression from infection to tuberculosis (TB) disease, TB mortality and TB recurrence, when being treated with metformin. However, a detailed mechanistic understanding of these protective effects is lacking. Here, we use mass cytometry to show that metformin treatment expands a population of memory-like antigen-inexperienced CD8⁺CXCR3⁺ T cells in naive mice, and in healthy individuals and patients with T2D. Metformin-educated CD8⁺ T cells have increased (i) mitochondrial mass, oxidative phosphorylation, and fatty acid oxidation; (ii) survival capacity; and (iii) anti-mycobacterial properties. CD8⁺ T cells from *Cxcr3*^{-/-} mice do not exhibit this metformin-mediated metabolic programming. In BCG-vaccinated mice and guinea pigs, metformin enhances immunogenicity and protective efficacy against *M. tuberculosis* challenge. Collectively, these results demonstrate an important function of CD8⁺ T cells in metformin-derived host metabolic-fitness towards *M. tuberculosis* infection.

¹ Singapore Immunology Network (SigN), Agency for Science, Technology and Research (A*STAR), Singapore 138648, Singapore. ² Department of Medicine, University of Massachusetts Medical School, 55 Lake Avenue North, Worcester, MA 01655, USA. ³ Fred Hutchinson Cancer Research Center, Seattle, WA 98109-1024, USA. ⁴ Department of Microbiology, Immunology & Pathology, Colorado State University, Fort Collins, CO 80525-1601, USA. ⁵ Department of Internal Medicine and Radboud Center for Infectious Diseases, Radboud University Medical Center, Nijmegen, Netherlands. ⁶ Gerontology Research Programme, Yong Loo Lin School of Medicine, Department of Psychological Medicine, National University Health System, National University of Singapore, Singapore, Singapore. ⁷ Department for Genomics & Immunoregulation, Life and Medical Sciences Institute (LIMES), University of Bonn, Bonn, Germany. ⁸ Lee Kong Chian School of Medicine, Nanyang Technological University, Singapore 308232, Singapore. ⁹ Translational Health Science and Technology Institute (THSTI), Faridabad, Haryana, India. ¹⁰ Infectious Disease Horizontal Technology Centre (ID HTC), Agency for Science, Technology and Research (A*STAR), Singapore 138648, Singapore. ✉email: Amit_Singhal@immunol.a-star.edu.sg

Tuberculosis (TB) is a major threat to global health owing to the inadequacies of antimicrobial treatment, the lack of a highly effective preventive or therapeutic vaccine, and the rise of drug-resistant *Mycobacterium tuberculosis* (*Mtb*) infection. Interest is now focused on a new therapeutic paradigm, host-directed therapies (HDT) for TB, to boost the antimicrobial efficacy of innate and adaptive immunity to TB while limiting excessive inflammation and tissue damage^{1,2}.

Patients with type 2 diabetes mellitus (T2D) have reduced risk of severe TB disease³ and *Mtb* infection when treated with metformin⁴. Metformin enhances the efficacy of anti-TB drugs, ameliorates lung pathology and reduces inflammation in *Mtb*-infected mice³. Retrospective data from eight clinical cohorts comprising a combined >250,000 individuals treated with metformin for T2D showed that metformin reduces the risk for progression to TB disease, mortality, lung cavitation, and relapse, and that it accelerates sputum conversion independently of glycemic control^{3–9}. Metformin is a top candidate in the TB-HDT pipeline, but a detailed mechanistic understanding of its protective immunometabolic benefits is lacking.

Although CD4⁺ T cells are generally recognized as the predominant effectors of adaptive immunity to TB, CD8⁺ T cells are also recognized to play a critical role in determining whether the *Mtb* infection is contained or progresses to active disease¹⁰. Upon infection, naive CD8⁺ T cells (T_N) differentiate into antigen (Ag)-specific effector T cells (T_E) and central memory T cells (T_{CM}). The latter have the ability to survive, expand, and generate cytotoxic CD8⁺ T_E cells upon encounter with a cognate Ag later in life¹¹. These T_{CM} are the major memory-like T cells in an infected or an immunized host. In contrast, in naive mice housed under specific-pathogen free conditions, Ag-inexperienced memory-like CD8⁺ T-cell (T_M) population, sometimes known as virtual-memory (T_{VM}) or innate-memory CD8⁺ T cells, have been described^{12–14}. These Ag-inexperienced CD8⁺ T_M cells (i) display unique and similar phenotypes to Ag-experienced CD8⁺ T_{CM} cells^{13–16}, (ii) rapidly respond to primary antigenic stimuli¹⁴, and (iii) mediate the protective immunity via non-canonical effector functions¹⁷.

Survival, activation, and effector function of T cells is fundamentally linked to cellular metabolic programming¹⁸. T_E cells predominantly use glycolysis, whereas T_{CM} cells use oxidative phosphorylation (OXPHOS) to meet energy demands^{18,19}. CD8⁺ T_{CM} exhibit increased mitochondrial fatty-acid oxidation (FAO), spare respiratory capacity (SRC), and biogenesis²⁰. SRC is the reserve capacity to produce energy in the mitochondria beyond the basal state. The increase in FAO required for optimal CD8⁺ T_{CM} generation and survival depends on the mitochondrial import of long chain fatty acids^{20,21}. Of note, CD8⁺ T_{CM} cells have been recently demonstrated to have lower SRC than CD8⁺ T_{VM} cells²².

In this study, we identify that metabolic reprogramming by metformin empowers CD8⁺ T cells to contain *Mtb* infection. We show that metformin treatment (i) expands memory-like CD8⁺ CXCR3⁺ T cells in naive mice and in healthy and diabetic humans, (ii) induces mitochondrial SRC and FAO in CD8⁺ T cells, and (iii) enhances Bacillus Calmette–Guérin (BCG) vaccine-elicited CD8⁺ T-cell responses and efficacy in mouse and guinea pig TB models. Metformin-educated Ag-inexperienced CD8⁺ T_M cells have gene expression signatures similar to an activated T cells, and restrict *Mtb* growth in T-cell-deficient mice.

Results

Metformin-educated CD8⁺ T cells restrict *Mtb* replication. We previously reported that metformin attenuates immunopathology and reprograms CD4⁺ and CD8⁺ T-cell responses in tissues of

Mtb-infected wild-type C57BL/6 (WT) mice³. To dissect the relative importance of metformin-educated CD4⁺ vs CD8⁺ T cells in TB defense, we compared their capacity to protect against *Mtb* infection in an adoptive transfer model. Splenic CD4⁺ or CD8⁺ T cells from WT mice treated with metformin or not (control group) were isolated and adoptively transferred into irradiated recipients, which were then infected with *Mtb* (Fig. 1a). Irradiated naive recipients that did not receive any T cells were also infected (no transfer group). In two independent experiments we found that mice which received metformin-educated CD8⁺ T cells had 0.5 log₁₀ reduced lung bacterial load at 21 days post infection (p.i.) compared with the mice that did not receive any T cells (Fig. 1b, c). At the same time, we noticed a 0.3 log₁₀ reduction in the lungs of mice receiving metformin-educated CD8⁺ T cells compared to those receiving CD8⁺ T cells from untreated mice (Fig. 1b, c). In these experiments, CD4⁺ T cells from metformin-treated and untreated donors failed to mediate the protection against *Mtb* (Fig. 1b, c).

The reduction in the lung bacterial load in recipients of metformin-educated (or metformin-primed) CD8⁺ T cells was paralleled by an increased frequency and total numbers of splenic memory CD8⁺CD44⁺CD62L⁺ T cells and naive CD8⁺CD44[−]CD62L⁺ T cells, and decreased effector CD8⁺CD44⁺CD62L[−] T cells compared to the mice that did not receive CD8⁺ T cells (Fig. 1d, e and Supplementary Fig. 1a). Of note, there was no change in the total number of CD3⁺, CD4⁺, and CD8⁺ T cells in the recipient mice among different groups (Supplementary Fig. 1b). These results suggested that the predominant effect of metformin treatment in donor mice was on the memory compartment of CD8⁺ T cells over effector compartment, as more memory cells were observed within the total CD8⁺ splenic T cells from *Mtb*-infected recipients receiving metformin-educated CD8⁺ T cells. In contrast, the proportions of memory to effector CD8⁺ T cells were equal in the spleens of *Mtb*-infected mice that received control CD8⁺ T cells (Fig. 1e). Mice receiving either metformin-educated or control CD8⁺ T cells had increased frequencies of perforin-expressing (Perforin⁺IFNγ[−]TNF[−]) memory CD8⁺ T cells compared with the mice that did not receive any T cells (Fig. 1f). In congenic recipients (receiving either metformin-educated or control CD8⁺ T cells) we saw similar increased numbers of Perforin⁺IFNγ[−] donor memory CD45.1⁺CD8⁺ T cells compared with the mice that did not receive any T cells (Fig. 1g and Supplementary Fig. 1c). Surprisingly, mice receiving metformin-educated CD8⁺ T cells had increased numbers of double- or triple-negative memory CD8⁺ T cells (Fig. 1f, g), indicating perforin-, IFNγ- and TNF-independent *Mtb* killing property of metformin-educated CD8⁺ T cells. CD4⁺ T cells have been reported to have such non-canonical anti-*Mtb* property²³. Overall, these results demonstrated the anti-*Mtb* activity of metformin-educated CD8⁺ T cells and suggested the potential of metformin to induce the expansion of memory CD8⁺ T cells with a unconventional effector phenotype.

Metformin expands CD8⁺CXCR3⁺ T_M cell population in naive mice.

To understand the effects of metformin exposure on CD8⁺ T cells in naive mice, we investigated the phenotype of metformin-educated splenic CD8⁺ T cells by mass cytometry (CyTOF)^{24,25} using a panel of 40 markers (Fig. 2a and Supplementary Table 1). Analysis of live CD45⁺CD19[−]TCRβ⁺CD90⁺CD4[−]CD8⁺ spleen cells (Supplementary Fig. 2a) using the nonlinear dimensionality reduction technique t-SNE with a machine-learning clustering algorithm (Phenograph) identified 20 distinct cell clusters with different expression characteristics of surface markers and intracellular transcription factors (Fig. 2b, c and Supplementary Fig. 2b). Based on the expression of CD62L and CD44, 20 clusters of CD8⁺ T cells were broadly classified

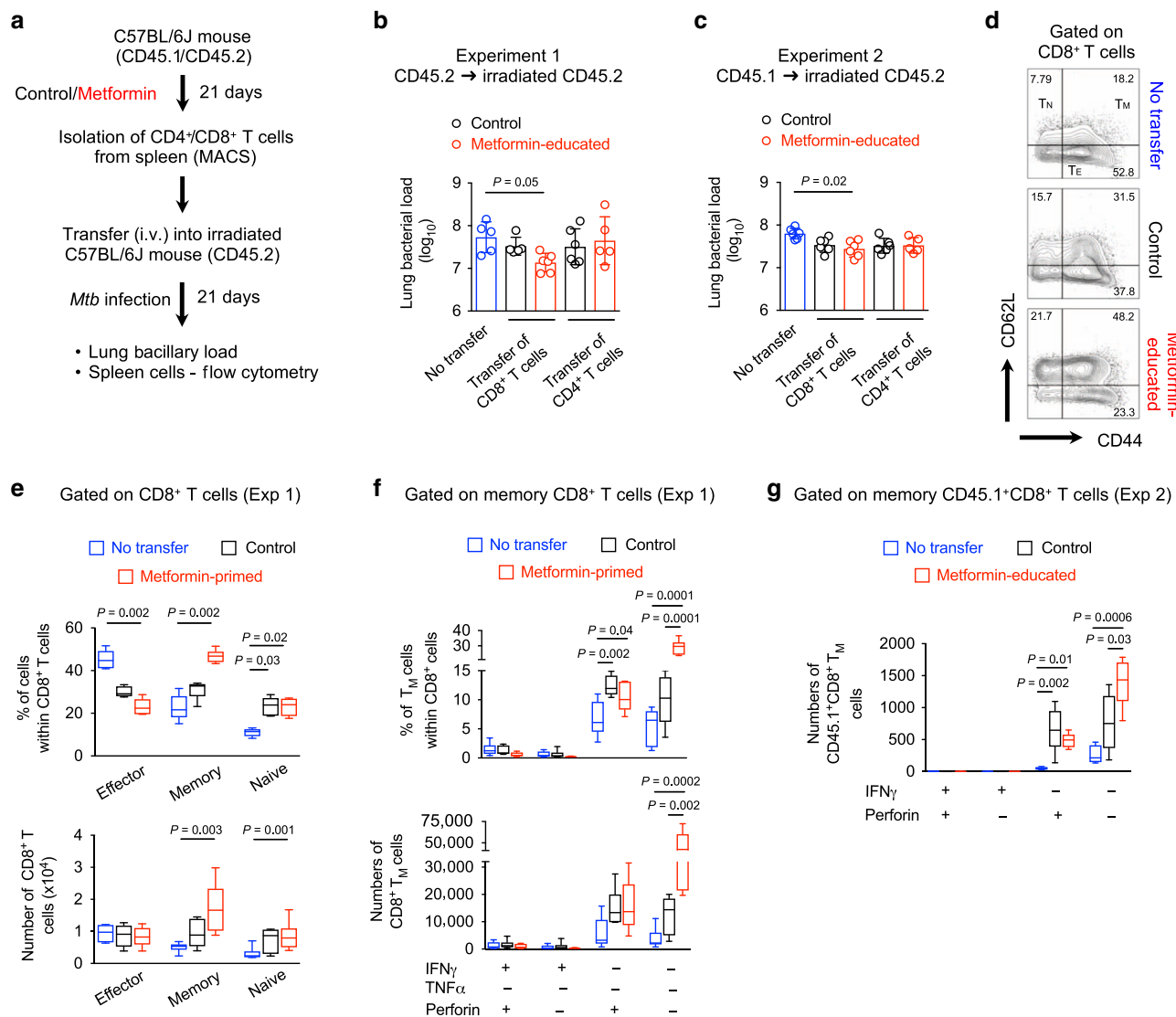
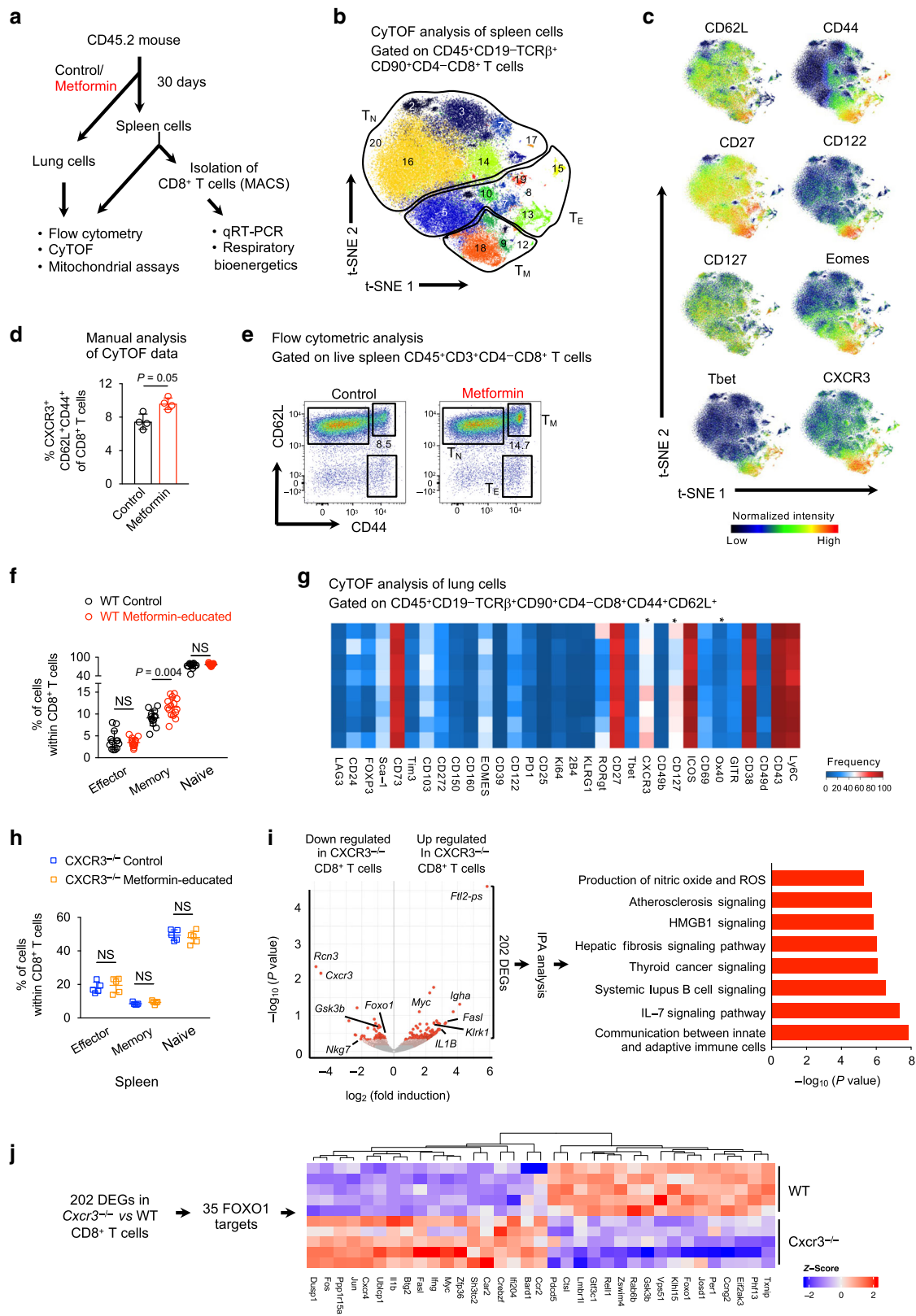


Fig. 1 Metformin-educated CD8⁺ T cells protect against *M. tuberculosis*. **a** Experimental strategy and assessed readouts. **b, c** Bacterial load in the lung of recipient mice 21 days post transfer, from two different experiments. No transfer—Irradiated recipients that did not receive any cells. Metformin-educated—CD4⁺ or CD8⁺ cells from donor mice treated with metformin; Control—cells from untreated mice. *n* = 5–6 mice/group/experiment. **d** Flow cytometric analysis of splenic CD8⁺ T cells from mice of experiment 1. T_M - memory T cells, CD44⁺CD62L⁺; T_E effector T cells, CD44⁺CD62L⁻; T_N - naive T cells, CD44⁻CD62L⁺. **e** Frequency and number of CD8⁺ T_E, T_M, and T_N cells in the recipient mice of experiment 1. *n* = 5 mice/group. **f** Frequency and number of IFN γ ⁺, TNF α ⁺, or Perforin⁺ CD8⁺ T_M cells from **e**. *n* = 5 mice/group. **g** Frequency and number of IFN γ ⁺ and/or Perforin⁺ CD45.1⁺CD8⁺ T_M cells in the recipient mice of experiment 2. *n* = 5 mice per group. Box-and-whisker plots show the median, 5 and 95 percentiles. All data are analyzed using Kruskal-Wallis test with Dunn’s multiple comparison.

into T_N, T_E, and T_M cells (Fig. 2b and Supplementary Fig. 2b). Automated machine-learning gating showed an expansion in the proportion of cells in clusters 9, 12 and 18, which comprised all T_M cells, within the total metformin-educated CD8⁺ T-cell population (Supplementary Fig. 2c). These clusters were strongly positive for conventional and unconventional memory T-cell markers including CD62L, CD44, CD127, CD27, CD122, and Eomes (Fig. 2c and Supplementary Fig. 2b). They also expressed Tbet, CXCR3 and CD49d (Fig. 2c and Supplementary Fig. 2b), indicating an effector phenotype and differentiating them from CD8⁺ T_{VM} cells^{15,26}. Tbet directly transactivates CXCR3²⁷ and retroviral-mediated CXCR3 expression in *Tbet*^{-/-} CD8⁺ T cells reconstitutes their ability to infiltrate inflamed tissues²⁸. CXCR3 plays an important role in T-cell trafficking and function²⁶ and expression of CXCR3 on CD8⁺ T_M cells is critical for populating the airways under steady state conditions²⁹.

Using a manual gating strategy, we validated the enrichment of CD8⁺ T_M cells identified by machine-learning strategy, confirming an increased frequency of memory-like CD8⁺CXCR3⁺ cells after metformin treatment (Fig. 2d). The enhanced CD8⁺ T_M frequency induced by metformin was further confirmed by flow cytometry of splenocytes from naive mice (Fig. 2e, f). Flow cytometric analysis also showed an enhanced frequency of total CD8⁺CXCR3⁺ cells in the spleen of metformin-treated naive mice (Supplementary Fig. 2d). Interestingly, OVA protein-stimulated CD8⁺ OT-I cells cultured with IL-15 (a cytokine known to stimulate T_M cell differentiation³⁰) showed increased T_{CM}/T_E ratio in the presence of metformin (Supplementary Fig. 3a, b), further demonstrating effectiveness of metformin in expanding the CD8⁺ T_{CM} compartment as well.

We next used CyTOF to decipher the heterogeneity in the lung CD8⁺ T cells from metformin-treated naive WT mice



(Supplementary Fig. 4a). Machine-learning analysis showed metformin-mediated increased expression of CXCR3 on lung (i) total CD8⁺ T cells (Supplementary Fig. 4b), (ii) CD8⁺ T_E cells (Supplementary Fig. 4c) and CD8⁺ T_M cells (Fig. 2g). This was further confirmed by manual gating of lung CyTOF data (Supplementary Fig. 4d) and flow cytometric analysis of lung cells

(Supplementary Fig. 4e) from metformin-treated naive mice. To test if CXCR3 was involved in the metformin-mediated expansion of CD8⁺ T_M cells in the spleen and lung, we compared untreated and metformin-treated *Cxcr3*^{-/-} mice. The *Cxcr3*^{-/-} mice had increased CD8⁺ T_E and reduced CD8⁺ T_M cells compared with WT mice in spleen (Fig. 2h) and lung (Supplementary Fig. 4f),

Fig. 2 Metformin treatment expands CD8⁺CXCR3⁺ T_M cell population in spleen and lungs of mice. **a** Experimental set-up of in vivo experiments. **b** Visualized t-SNE map of CD8⁺ T cells from spleen of wild-type (WT) mice with automated cluster gating. t-SNE was performed on live CD45⁺CD90⁺TCRαβ⁺CD4⁻CD8⁺ cells after gating out B cells. **c** Normalized expression intensities of indicated marker was calculated and overlaid on the t-SNE plot, characterizing all clusters of CD8⁺ T cells in spleen. Means ± SD of four mice per group, one-tailed Mann-Whitney *U* test. **d** Manual gating analysis of CD8⁺CXCR3⁺ T_M cells in control and metformin-treated WT mice. **e, f** Flow cytometric analysis of splenic CD8⁺ T-cell subsets from control and metformin-treated WT mice. Pooled data from three independent experiments. Means ± SD of *n* = 13–15 mice per group, two-tailed Mann-Whitney *U* test. **g** Heat map displaying frequency of various surface markers in lung CD8⁺ T cells of control and metformin-treated WT mice. *n* = 4. **p* ≤ 0.05 by two-tailed paired *t* test. **h** Flow cytometric analysis of spleen CD8⁺ T_E, T_M, and T_N cells of control and metformin-treated *Cxcr3*^{-/-} mice. Data shown one out of two experiments, mean ± SD of five mice per group. **i** Left—volcano plot showing DEGs from RNA sequencing data of CD8⁺ T cells from *Cxcr3*^{-/-} and WT mice. *n* = 5 mice/group. Right—Canonical pathway enrichment via Ingenuity pathway analysis (IPA) of 202 DEGs. **j** Heat map displaying the expression level of 35 FOXO1 targets in data shown in **i**. NS not significant.

confirming an earlier report³¹, while in the present study metformin treatment did not alter the percentage of T_E, T_M, or T_N cells in *Cxcr3*^{-/-} mice.

To determine why metformin failed to expand CD8⁺ T_M cells in *Cxcr3*^{-/-} mice, we performed RNA sequencing (RNAseq) on splenic CD8⁺ T cells from *Cxcr3*^{-/-} and WT mice. We found 202 differentially expressed genes (DEGs) in CD8⁺ T cells from *Cxcr3*^{-/-} compared with WT mice (Fig. 2i, left panel and Supplementary Data 1). Ingenuity pathway analysis (IPA) of these DEGs revealed an enrichment of genes associated with communication between innate and adaptive immune cells and IL-7 signaling pathway (Fig. 2i, right panel and Supplementary Table 2). For optimal CD8⁺ T_M cell homeostasis a discontinuous IL-7 signaling has been proposed³². Among DEGs, we found downregulation of *Foxo1* (Forkhead Box O1), *Gsk3b* (Glycogen synthase kinase 3 beta) and *Nkg7* (Natural killer cell granule protein 7, a cytotoxic marker), and upregulation of *Myc*, *Jun*, and *Il1b* (Interleukin 1 beta; Supplementary Data 1). Importantly, FOXO1, GSK3B, and *Myc* are required in the maintenance of memory state of CD8⁺ T cells^{33–35}. Further analysis of DEGs revealed a significant enrichment of FOXO1 targets (*n* = 35)³⁶ among 202 DEGs (Fig. 2j, *P* = 1.2 × 10⁶, hypergeometric test, see “Methods”), indicating a perturbation in FOXO1 signaling in CD8⁺ T cells from *Cxcr3*^{-/-} mice. Taken together, our data suggested that metformin reprograms the CD8⁺ T cells phenotype and shapes the generation of the CD8⁺CXCR3⁺ T_M population. This generation of CD8⁺CXCR3⁺ T_M cells could be mediated by FOXO1, which can also control CD8⁺ T_M responses during infection³⁷.

Metformin promotes CD8⁺ T-cell SRC and mitochondrial health. Enrichment of CD8⁺ T_M cells by metformin suggested an effect dependent on the regulation of cellular metabolism. Therefore, we measured the bioenergetic profiles of spleen CD8⁺ T cells from untreated and metformin-treated naive WT mice. Oxygen consumption rate (OCR), an indicator of OXPHOS, was higher in metformin-treated CD8⁺ T cells compared to untreated CD8⁺ T cells (Fig. 3a). Importantly, metformin-treated CD8⁺ T cells demonstrated a larger mitochondrial SRC when compared with CD8⁺ T cells from untreated mice (Fig. 3a). This increase in SRC was found to be dependent on CXCR3 expression (Fig. 3b). The absence of metformin-mediated increased OXPHOS in CD8⁺ T cells from *Cxcr3*^{-/-} mice could be owing to the inherent reduced expression of *Foxo1* in these cells (Fig. 2i). Of note, FOXO1 regulates oxidative stress responses, proliferation, cell survival, and apoptosis, and connects metabolic activity with immune response^{38–40}.

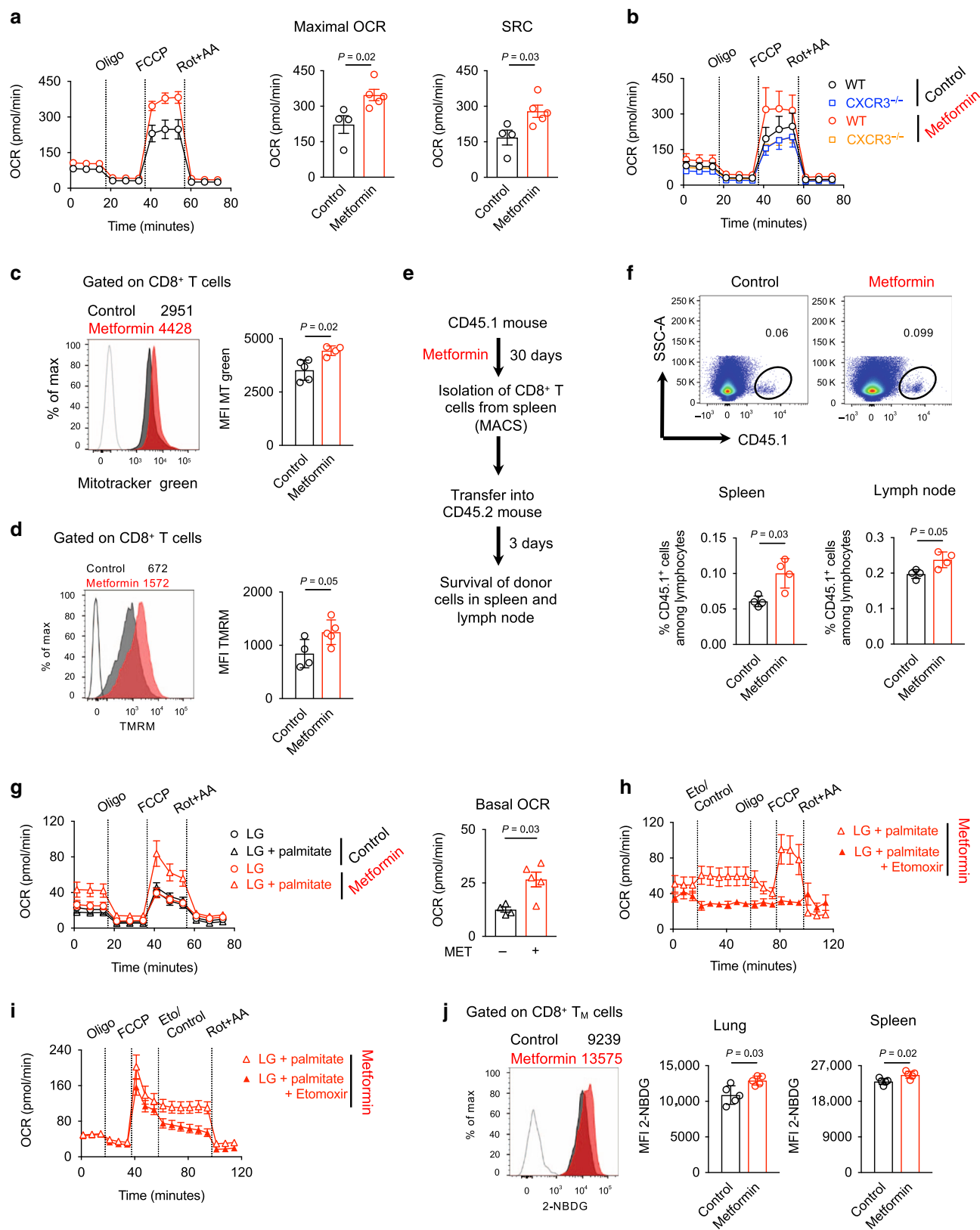
Enhanced SRC in cells might be explained by increased cellular mitochondrial mass²⁰. CD8⁺ T cells from metformin-treated WT mice showed increased Mitotracker Green median fluorescence intensity (MFI) compared with CD8⁺ T cells from untreated mice, indicating increased mitochondrial mass (Fig. 3c and

Supplementary Fig. 5a). Metformin-educated CD8⁺ T cells from WT mice also showed a trend of increased mRNA expression for *Sell* (*CD62L*), *Cpt1a* and *Tfam* (mitochondrial transcription factor A) genes (Supplementary Fig. 5b). In addition, metformin-educated CD8⁺ T cells showed increased accumulation of tetramethylrhodamine, methyl ester (TMRM), indicating healthy and functional mitochondria (Fig. 3d).

Metformin promotes survival of CD8⁺ T cells. To further assess the impact of metformin on the CD8⁺ T_M compartment, we characterized the survival capacity of CD8⁺ T cells in vivo by adoptively transferring metformin-treated or untreated cells into congenic mice (Fig. 3e). After 3 days, we found significantly more CD45.1⁺ donor metformin-treated CD8⁺ T cells in spleen and lymph node of the recipient mice (Fig. 3f). Together, our data suggested that metformin enhanced mitochondrial SRC and health of CD8⁺ T cells and promoted their survival, which are characteristic features of T_M cells.

Metformin-educated CD8⁺ T cells use glucose for FAO and OXPHOS. As metformin promoted the enrichment of the CD8⁺ T_M cells (Fig. 2) with increased SRC (Fig. 3a), we reasoned that metformin-educated CD8⁺ T cells might utilize extracellular glucose to fuel mitochondrial FAO and OXPHOS, a property of IL-15-induced CD8⁺ T_M cells²⁰. We evaluated this by measuring OCR in CD8⁺ T cells cultured in low glucose (LG) medium. The increased OCR and SRC seen in CD8⁺ T cells from metformin-treated mice cultured in glucose-sufficient medium (25 mM, Fig. 3a) was not observed under LG conditions (0.5 mM, Fig. 3g). This suggested that glucose was driving FAO and OXPHOS in metformin-educated CD8⁺ T cells. In addition, under LG conditions, supplementation with fatty acid (palmitate) rescued the SRC of metformin-educated CD8⁺ T cells (Fig. 3g), indicating that increased SRC of metformin-educated CD8⁺ T cells in glucose-sufficient media (Fig. 3a) was derived from FAO.

Next, we used the CPT1a inhibitor etomoxir (Eto), which blocks mitochondrial FAO, to confirm that the enhanced SRC in CD8⁺ T cells from metformin-treated mice depended on FAO. Treatment with Eto, either before or after carbonylcyanide-*p*-trifluoromethoxyphenylhydrazone (FCCP) injection, impaired basal OCR and SRC, respectively, in metformin-educated CD8⁺ T cells (Fig. 3h, i). As CPT1a-independent effects of Eto on mitochondrial respiration have been observed⁴¹ and we used higher concentration of Eto (viz. 200 μM), FAO independent effect of metformin on OXPHOS cannot be ruled out. To further support the hypothesis that metformin-educated CD8⁺ T_M cells used glucose for FAO and OXPHOS, we performed glucose uptake assay using the fluorescent glucose analog 2-NBDG. Lung and spleen CD8⁺ T_M cells from metformin-treated mice acquired more 2-NBDG than CD8⁺ T_M cells from untreated mice (Fig. 3j). We did not find an increased uptake of 2-NBDG by CD8⁺ T_E



cells from metformin-treated mice (Supplementary Fig. 5c), indicating minimal effect of metformin on the metabolic reprogramming of those cells. Together, our data suggested that glucose fuels mitochondrial FAO, which might be responsible for the induction of OXPHOS in metformin-educated CD8⁺ T cells.

Distinct gene expression in metformin-educated CD8⁺ T_M cells. We next used RNAseq to characterize the effect of metformin on splenic CD8⁺ T_M cells (Fig. 4a). A total of 267 genes were found to be differentially expressed in metformin-educated CD8⁺ T_M cells (Fig. 4a and Supplementary Data 2). IPA-based molecular function enrichment revealed an effect of metformin

Fig. 3 Metformin promotes CD8⁺ T-cell SRC, mitochondrial mass, survival, and FAO. **a** Oxygen consumption rate (OCR) and spare respiratory capacity (SRC) in spleen CD8⁺ T cells from control and metformin-treated WT mice in response to different drugs. $n = 4$ control mice, $n = 5$ metformin-treated mice. **b** OCR in spleen CD8⁺ T cells from control and metformin-treated *Cxcr3*^{-/-} mice. $n = 6$ mice/group. **c** Mitotracker green staining of CD8⁺ T cells from control and metformin-treated WT mice. *MFI* - median fluorescence intensity. $n = 4$ mice/group. **d** TMRM staining of CD8⁺ T cells from control and metformin-treated WT mice. $n = 4$ mice/group. **e** Experimental schematic of adoptive transfer of CD8⁺ T cells into congenic WT mice. **f** Frequency of CD45.1⁺ cells in the spleen and lymph node of recipient mice. $n = 4$ mice/group. **g** OCR in spleen CD8⁺ T cells from control and metformin-treated WT mice in response to different drugs under low glucose (LG) condition in the presence and absence of palmitate. $n = 5$ mice/group. **h, i** OCR in spleen CD8⁺ T cells from metformin-treated WT mice in response to different drugs under LG condition in the presence of palmitate. **h** $n = 5$ mice/group; **i** $n = 8$ mice/group. **j** Glucose uptake (2-NBDG) in CD8⁺ T_M cells, analyzed by flow cytometry. $n = 5$ mice/group. Data in **a, c, d, f, g,** and **j** are presented as mean \pm SD, two-tailed Mann-Whitney *U* test.

on the expression of 86 genes associated with cell survival (Fig. 4b and Supplementary Table 3). Among these 86 genes we found an upregulation of *Cdk1* (cyclin-dependent kinase 1) and *Agap2* (Arf-GAP with GTPase, ANK repeat and PH domain-containing protein 2) genes, consistent with a role of metformin in modulating CD8⁺ T_M cell fate (Fig. 4c). In addition, metformin reduced the expression of *Mtor* (mammalian target of rapamycin), *Immt* (inner membrane mitochondrial protein, mitofilin), and *Casp1* (caspase-1) genes (Fig. 4c). Metformin is known to inhibit mTOR⁴², whereas IMMT deficiency has been associated with perturbed mitochondrial function⁴³. As caspase-1 is required for pyroptosis, a form of programmed cell death⁴⁴, we reasoned that the enhanced survival of metformin-educated CD8⁺ T cells (Fig. 3f) might be explained by the reduced caspase-1 activity. As predicted, metformin-treated *Mtb*-infected mice had reduced numbers of CD8⁺caspase-1⁺ cells in the spleen compared to the untreated *Mtb*-infected mice (Fig. 4d).

To test whether metformin-educated CD8⁺ T_M cells survived better in vivo under infection settings, we adoptively transferred flow-sorted CD8⁺ T_M cells into congenic *TCRβδ*^{-/-} mice that were subsequently infected with *Mtb* or BCG (Fig. 4e; total three experiments). We found significantly more metformin-educated donor cells in the lungs (Fig. 4f) and spleens (Fig. 4g) of the recipient *Mtb*-infected *TCRβδ*^{-/-} mice. This paralleled with a trend for lower bacterial load in the lungs of *Mtb*-infected *TCRβδ*^{-/-} mice that received metformin-educated CD8⁺ T_M cells compared with those receiving control CD8⁺ T_M cells (1.4 log₁₀ reduction), although this did not reach statistical significance (Fig. 4h). In other experiments, *TCRβδ*^{-/-} mice receiving metformin-educated CD8⁺ T_M cells had significantly lower lung and spleen bacterial load compared with the *TCRβδ*^{-/-} mice that did not receive any T cells (0.9–1.3 log₁₀ reduction; Fig. 4i, j). In this experiment, CD8⁺ T_E cells from control and metformin-treated mice equally restricted lung bacterial loads in the *TCRβδ*^{-/-} recipient mice to a comparable level (Fig. 4i). Collectively, our data indicated that metformin reprogrammed gene expression of CD8⁺ T_M cells, increasing their survival and anti-mycobacterial properties.

Metformin enhances BCG vaccine immunogenicity and efficacy.

The generation of T_M cells has important implications for vaccine efficacy. As metformin-educated CD8⁺ T_M cells display distinct phenotypes and function associated with host protection, we evaluated the effect of metformin on the response to vaccination with BCG (Supplementary Fig. 6a). In BCG-vaccinated mice, metformin treatment was associated with an increased frequency of PPD (purified protein derivative of *Mtb*)-specific IFN γ -secreting splenic CD8⁺ T cells (Fig. 5a) but not CD4⁺ T cells (Supplementary Fig. 6b), compared with untreated BCG-vaccinated animals. Similar trend was observed in PPD-specific CD8⁺ T_M and T_E cells from metformin-treated BCG-vaccinated mice (Fig. 5a). We also observed an increased frequency of IFN γ ⁺ total CD8⁺ cells (unstimulated) from metformin-treated BCG-vaccinated mice (Fig. 5a). CD8⁺ T cells from metformin-treated BCG-vaccinated

mice also demonstrated an increased mitochondrial mass (Fig. 5b) and health (Fig. 5c) similar to that seen in unvaccinated animals (Fig. 3b, c). We next performed RNAseq on flow-sorted CD8⁺ T_M cells from metformin-treated and untreated BCG-vaccinated mice. Comparative analysis revealed 607 DEGs that were enriched for genes associated with OXPHOS (Fig. 5d, Supplementary Data 3 and Supplementary Table 4). A heat map of OXPHOS genes showed an increased expression of electron transport chain genes in CD8⁺ T_M cells from metformin-treated BCG-vaccinated mice (Supplementary Fig. 6c).

We next examined whether metformin treatment would enhance BCG vaccine-mediated *Mtb* control in mice. A trend for reduced *Mtb* bacillary load in the lungs of metformin-treated vaccinated mice compared to untreated vaccinated mice was observed (Fig. 5e). BCG-vaccinated metformin-treated mice showed an increased frequency of memory CD8⁺ T cells, and decreased effector CD8⁺ T cells upon *Mtb* infection compared to the BCG-vaccinated mice alone (Supplementary Fig. 6d, upper panel). When stimulated with class I-restricted peptide (TB10.4) of the *Mtb* *EsxH* gene, memory CD8⁺ T cells from BCG-vaccinated metformin-treated mice demonstrated increased TNF production compared to the BCG-vaccinated mice alone (Supplementary Fig. 6d, lower panel). We next used the guinea pig TB model to further evaluate metformin-mediated enhancement of BCG efficacy (Fig. 5f)⁴⁵. Lung *Mtb* bacillary load in metformin-treated BCG-vaccinated guinea pigs was significantly lower compared to unvaccinated animals or animals which received only metformin, reduction of 3.4 log₁₀ and 2.9 log₁₀, respectively (Fig. 5g). In this experiment, bacillary load in untreated vaccinated animals was not significantly different from unvaccinated animals (reduction of 0.4 log₁₀, Fig. 5g). Histopathological evaluation of the infected lungs showed reduced infiltrating leukocytes and lesions in BCG-vaccinated guinea pigs compared with unvaccinated animals (4.3-fold reduction in lung lesion burden, Fig. 5h). Importantly, lungs of metformin-treated BCG-vaccinated guinea pigs showed 11.2- and 2.6-fold reduced lesion burden compared with the control and untreated BCG-vaccinated guinea pigs, respectively (Fig. 5h, i). Taken together, our data suggested that metformin enhances the BCG vaccine response and efficacy against *Mtb*.

Metformin expands CD8⁺CXCR3⁺ T_M cell population in humans.

To investigate the effect of metformin in humans, we performed CyTOF on peripheral blood mononuclear cells (PBMCs) from healthy human participants who took a standard dose of metformin for five days (Fig. 6a, See Methods)⁴⁶. The PBMCs were stained with a panel of 38 markers (Supplementary Table 5). Analysis of CD8⁺ T cells (CD45⁺CD14⁻CD19⁻HLA-DR⁺CD3⁺CD4⁻γδTCR⁻TCRVα7.2⁻CD161⁻CD56⁻CD8⁺) using t-SNE (Supplementary Fig. 7a) identified T_N cells (CCR7⁺CD45RO⁻CD45RA⁺), T_E cells (CCR7⁻CD45RO⁺CD45RA⁺) and T_M cells (CCR7⁺CD45RO⁺CD45RA⁻) (Fig. 6b, c; Supplementary Fig. 7a)⁴⁷. Two distinct T_M and T_E subgroups were observed (Fig. 6b).

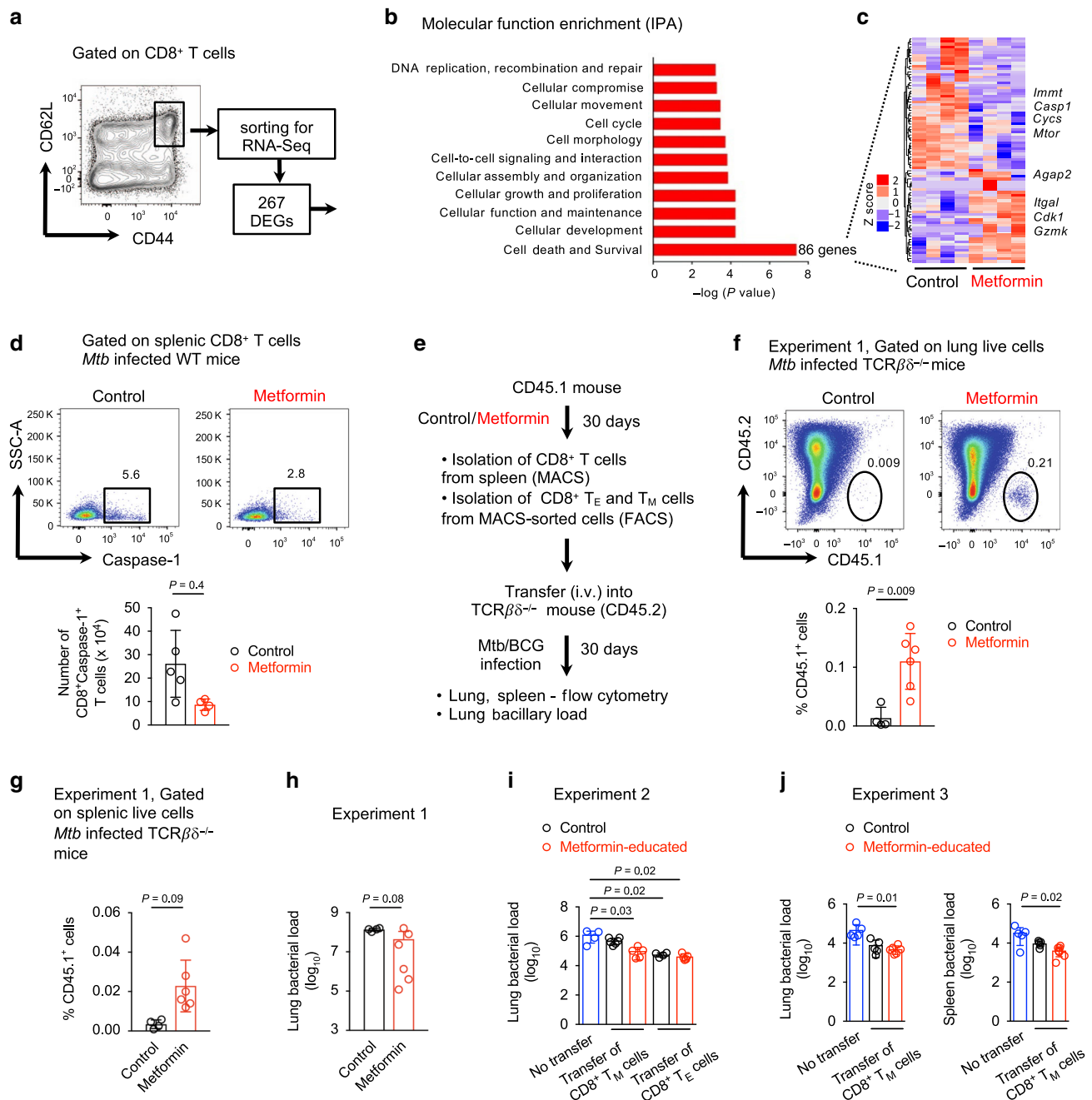


Fig. 4 Metformin reprograms gene expression of CD8⁺ T_M cells. **a** Schematic depicting sorting of CD8⁺ T_M cells for RNA sequencing and identification of DEGs in metformin-educated CD8⁺ T_M cells. **b** Molecular function enrichment via Ingenuity pathway analysis (IPA) of DEGs in **a**. **c** Heat map displaying the expression level of 86 genes related to cell death and survival. **d** Flow cytometric analysis of caspase-1 in splenic CD8⁺ T cells from *Mtb*-infected mice treated or not with metformin. $n = 5$ mice/group. **e** Experimental set-up for the transfer of CD8⁺ T_M or T_E cells into *TCRβδ*^{-/-} mice followed by *Mtb* or BCG infection. Three experiments were performed. **f, g** Flow cytometric analysis of the frequency of CD45.1⁺ lung **f** and splenic **g** cells in recipient mice. $n = 4$ control group, $n = 6$ metformin group. **h** Bacterial load in the lung of *Mtb*-infected *TCRβδ*^{-/-} recipient mice. **i, j** Bacterial load in the lung of BCG-infected *TCRβδ*^{-/-} recipient mice. Data of mean \pm SD of 4–5 mice per group, Kruskal–Wallis test with Dunn’s multiple correction. Data in **d, f, g**, and **h** is presented as mean \pm SD, two-tailed Mann–Whitney *U* test.

Interestingly, the T_{M2} subset was positive for CD127 and CXCR3 (Fig. 6d), similar to what we observed in mouse CD8⁺ T_M cells (Fig. 2c). This CD8⁺ T_{M2} (CD8⁺CD127⁺CXCR3⁺) population expanded upon metformin intake in healthy subjects (Fig. 6e), and also showed increased expression of anti-apoptotic BCL2 (Fig. 6f), which was previously shown to correlate with CD8⁺ T-cell survival⁴⁸. We next performed flow cytometric analysis on the PBMCs from T2D patients who were being treated with either metformin or

with other anti-diabetic drugs as monotherapy (Supplementary Fig. 7b and Supplementary Table 6). These two groups had similar fasting plasma glucose levels (Supplementary Table 6). Metformin-receiving T2D patients showed an increased frequency of CD8⁺ CXCR3⁺ T_M cells compared with T2D patients treated with other anti-diabetic drugs (Fig. 6g). Overall, our data indicated that metformin induced the expansion of memory-like CD8⁺CXCR3⁺ T cells both in mice and humans.

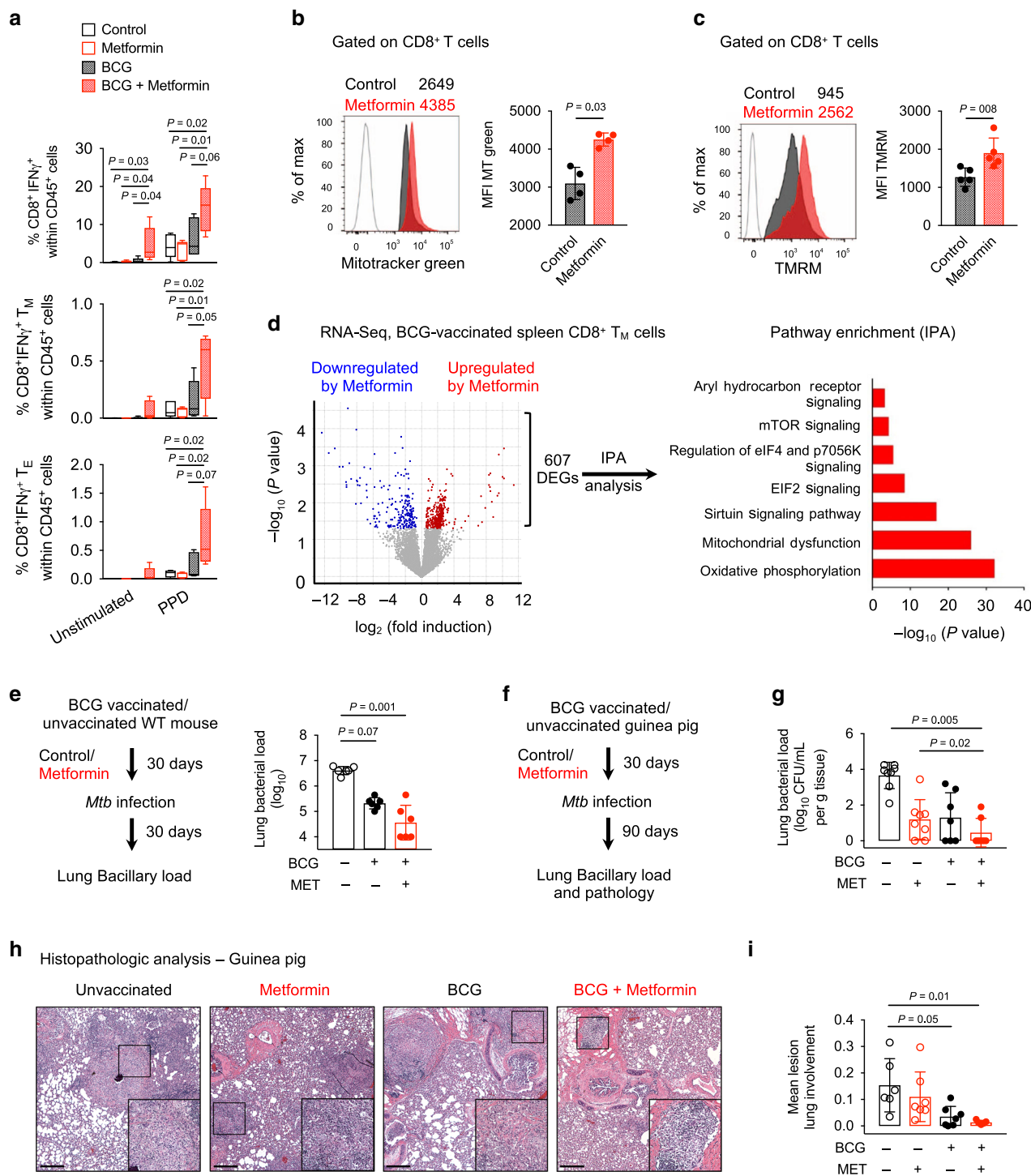


Fig. 5 Metformin promotes BCG vaccine immunogenicity and efficacy. **a** PPD-specific response of spleen cells, analyzed by flow cytometry. Data on IFN γ producing CD8⁺ T, T_M, and T_E cells. $n = 5$ mice/group. Box-and-whisker plot show the median, 5 and 95 percentiles, one-way ANOVA with Turkey’s multiple comparison test. **b, c** Mitotracker green **b** TMRM **c** staining of splenic CD8⁺ T cells from control and metformin-treated BCG-vaccinated WT mice. **b** $n = 4$ mice/group; **c** $n = 5$ mice/group. means \pm SD, Mann–Whitney U test. **d** Changes in gene expression in CD8⁺ T_M cells from BCG-vaccinated mice treated or not with metformin. IPA analysis of 607 DEGs. $n = 5$ mice/group. **e** Schematic of *Mtb* infection of metformin-treated BCG-vaccinated mice. Lung bacillary load at 30 days post infection (p.i) is shown. $n = 6$ mice/group. **f** Schematic of *Mtb* infection of metformin-treated unvaccinated and BCG-vaccinated guinea pigs. **g** Lung bacillary load in unvaccinated and BCG-vaccinated *Mtb*-infected guinea pigs treated or not with metformin. $n = 6$ –7 animals/group. **h** Light micrographs of hematoxylin and eosin (H&E) staining of lung sections from animals in **g**. Magnification for main image $\times 40$ (scale bars, 50 μ m) and insert $\times 100$. **i** Morphometric analysis of lung sections shown in **h** indicating the mean lesion lung involvement from each guinea pig. $n = 6$ –7 animals/group. Data in **a**–**c**, **e** is representative of two independent experiments. Guinea pig data in **g** and **i** is from one experiment. Data in **e**, **g**, and **i**, means \pm SD, Kruskal–Wallis test with Dunn’s multiple correction.

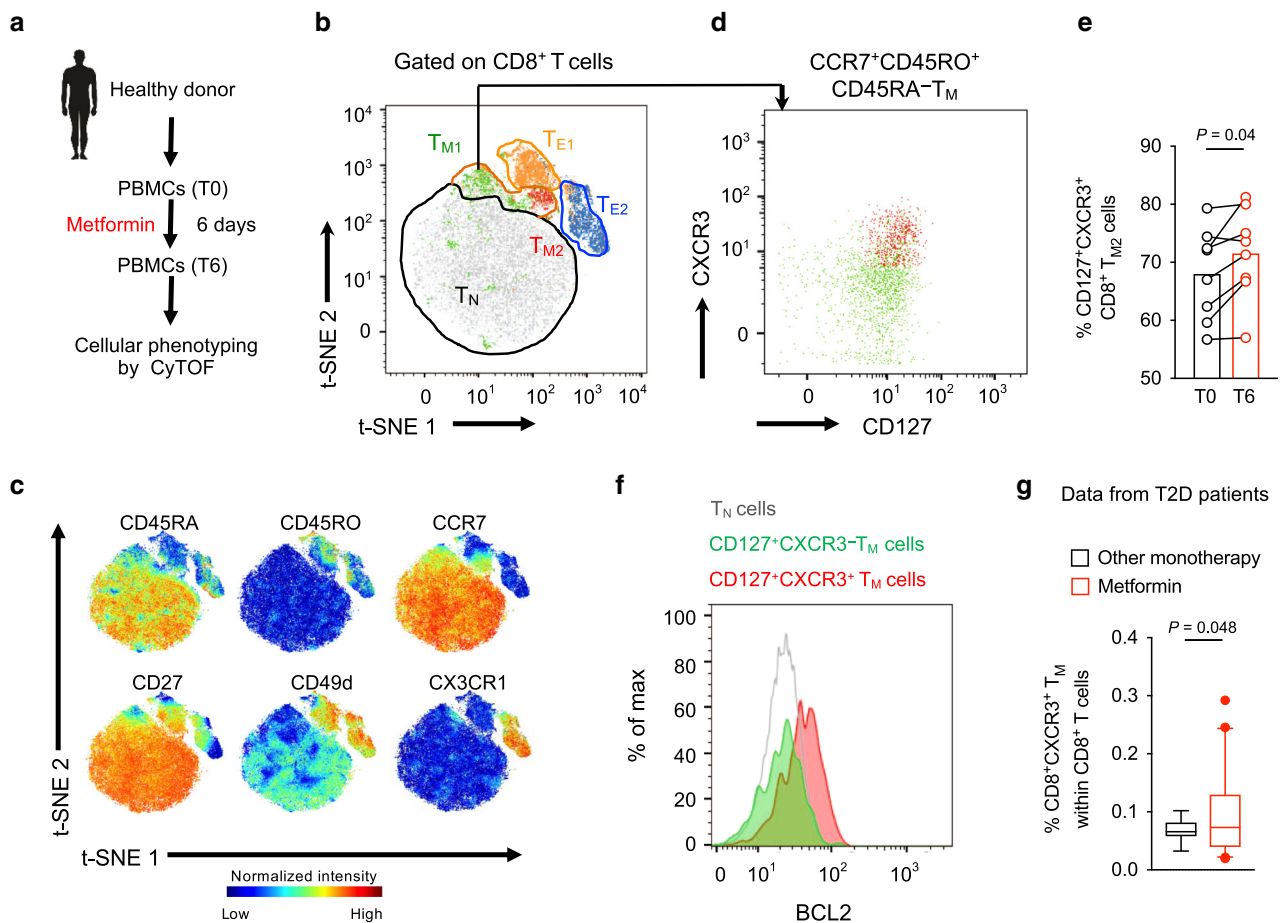


Fig. 6 Metformin treatment expands CD8⁺CXCR3⁺ T_M cell population in humans. **a** Strategy of analyzing PBMCs from metformin-treated healthy individuals. **b** t-SNE map of human peripheral CD8⁺ T cells with manually cluster gating for T_E, T_M, and T_N cells. **c** Normalized expression intensities of indicated markers were calculated and overlaid on the t-SNE plot, characterizing all cluster of human CD8⁺ T cells. **d** Manual gating identified differential expression of CD127 and CXCR3, distinguishing two CD8⁺ T_M subpopulations, T_{M1} and T_{M2}. **e** Frequency of CD8⁺CD127⁺CXCR3⁺ T_M cells before and after metformin treatment. *n* = 8 subjects, analysis by Wilcoxon matched-pairs signed rank test. **f** Overlay plot showing expression of BCL2 in CD8⁺CD127⁺CXCR3⁻ and CD8⁺CD127⁺CXCR3⁺ T_M cells. BCL2 expression in CD8⁺ T_N cells is also indicated. Data shown from one representative donor. **g** Flow cytometric analysis of frequency of peripheral CD8⁺CXCR3⁺ T_M cells in T2D patients receiving either metformin or other diabetic monotherapy, *n* = 18 other monotherapy group, *n* = 42 metformin group. Box-and-whisker plot show the median, 5 and 95 percentiles. Analysis by two-tailed *t* test with Welch's correction.

Effect of metformin on *Mtb* clearance and reactivation. CD8⁺ T cells play an important role in long-term protective immune responses against *Mtb* infection and reactivation of latent TB^{10,49}. To assess the persistence of metformin effects, we first measured the bioenergetic profiles of splenic CD8⁺ T cells from naive mice that received metformin for 6 months. Similar to our previous finding (Fig. 3a), OCR was higher in CD8⁺ T cells from mice chronically treated with metformin compared with those from untreated mice (Supplementary Fig. 8a). This was associated with an increased number of splenic CD8⁺ T_M cells in metformin-treated mice (Supplementary Fig. 8b). We next used a modified version of the TB Cornell model⁵⁰ to evaluate the long-term effects of metformin on *Mtb* clearance and reactivation. In this model, *Mtb*-infected mice were treated with pyrazinamide (PZA) and isoniazid (INH) ± metformin for 70 days starting on day 40 p.i., followed by a rest period of 40 days, and then challenged with dexamethasone to reactivate any persisting bacilli (Supplementary Fig. 8c). In the animals which received metformin along with PZA and INH, bacilli was recovered from the lungs of 40–50% mice sacrificed 40 days after the drugs were stopped (day 150 p.i., Table 1 and Supplementary Fig. 8c). However for mice which received only PZA and INH, bacilli were recovered from 75–80%

Table 1 Efficacy of metformin against *Mtb* in modified Cornell-mice model.

Exp no.	Day 150		Day 167	
	PZA+INH [‡]	MET+PZA+INH [‡]	PZA+INH	MET+PZA+INH
Exp 1	1/5 (20%)	3/5 (60%)	1/5 (20%)	4/5 (80%)
Exp 2	1/4 (25%)	2/4 (50%)	1/4 (25%)	2/4 (50%)

Proportion of mice with no detectable CFUs in the lungs and spleen during PZA+INH therapy with and without MET in two different experiments. INH isoniazid, PZA pyrazinamide, MET metformin.

[‡]*Mtb*-infected mice were administered INH (10 µg/mL) and PZA (15 mg/mL).

^{||}Number of mouse with no detectable CFU out of total number of animals in that group. In bracket percentage information is provided.

of animals at day 150 p.i. After 15 days of dexamethasone treatment bacilli were recovered from the lungs of 20–50% of mice treated with metformin+PZA +INH compared with 75–80% mice treated with PZA + INH (Table 1). Taken together, these data suggest that metformin enhances the sterilizing activity

of suboptimal antimicrobial treatment for *Mtb* infection by boosting intrinsic host immune function.

Discussion

The goals of HDT for TB are to accelerate lesion sterilization and mitigate immune pathology by educating host anti-*Mtb* responses^{2,51}. Previously, we proposed metformin as an adjunctive TB treatment, reporting that it lowers risk for cavitary TB and mortality in adults with T2D³. In the present study, we showed that metformin treatment (i) expands CD8⁺CXCR3⁺ T_M cells in mice and humans, (ii) reprograms CD8⁺ T cells metabolic and transcriptional circuits, (iii) enhances BCG vaccine protective efficacy, and (iv) improves sterilizing ability of antibiotics, thus preventing *Mtb* reactivation.

Metformin-educated Ag-inexperienced CD8⁺CXCR3⁺ T_M cells share phenotypic and functional properties with Ag-specific CD8⁺ T_{CM}, Ag-inexperienced T_{VM}, innate-memory CD8⁺ T, and/or IL-15-derived CD8⁺ T_M cells⁵², and have enhanced survival and anti-*Mtb* properties. Cytokine-activated CD8⁺ T_M cells are known to contribute to host protection against diverse pathogens¹⁷. The differential transcriptomic and phenotypic properties of metformin-educated CD8⁺CXCR3⁺ T_M cells suggest that these cells may represent another type of “innate CD8⁺ T-cell”¹⁷. The CXCR3/CXCL10 axis can shape the distribution of CD8⁺ T_M cells in the tissues of non-immunized mice⁵³ and CXCR3-expressing innate CD8⁺ T_M cells are known to express activation markers, respond to IL-2 and IL-15, and possess antibacterial effector function^{54,55}. In addition, CXCR3 is required for the migration and establishment of CD8⁺ T_{CM} cell population in the respiratory tract, where they protect against influenza A virus infection²⁹.

CD8⁺ T_M cells protect the host against infectious diseases by virtue of their recall ability to expand and execute effector functions^{10,56}. These responses are promoted by AMP-activated protein kinase (AMPK)⁵⁷, a crucial energy sensor and an indirect target of metformin. AMPK signaling promotes OXPHOS during CD8⁺ T_M generation⁵⁸ and maintains mitochondrial health in T_M cells⁵⁹. This indicates the importance of AMPK and OXPHOS in rewiring of metformin-educated Ag-inexperienced CD8⁺ T_M cells in our experiments. We demonstrated that CXCR3 signaling is required for metformin-mediated induction of OXPHOS in CD8⁺ T cells, suggesting a possible CXCR3- and AMPK-dependent effect(s). How CXCR3 regulates metformin-mediated induction of OXPHOS, mitochondrial health and expansion of CD8 memory remains to be determined. Interestingly, mice devoid of AMPK in CD4⁺ T cells shows deficiency in the CXCR3 expression⁶⁰. Our transcriptomic analysis of CD8⁺ T cells from *Cxcr3*^{-/-} mice suggested dependency of metformin-mediated reprogramming of mitochondrial function on Foxo1 network (Fig. 2i, j), which is an important metabolic check point⁴⁰. Of note, TB immunopathology could be modulated by targeting T cells mitochondrial metabolism⁶¹.

The recall ability of T_M cells is also the basis for vaccinations against numerous diseases including TB. The current TB vaccine, BCG, is unable to protect against pulmonary TB in adults, hence there is an urgent need to improve BCG or to develop new TB vaccine. Here we showed that metformin treatment resulted in an increased (i) elicitation of Ag-specific CD8⁺ T_{CM} in the tissues of BCG-vaccinated mice, (ii) TNF secreting Ag-specific CD8⁺ T_{CM} cells in the tissues of BCG-vaccinated *Mtb*-challenged mice, and (iii) protection of BCG-immunized mice and guinea pig against *Mtb* challenge. Importantly, expression of CXCR3 by TB vaccine-specific CD8⁺ T cells is needed for their homing to the lung mucosa⁶². This raises the possibility of the presence of metformin-educated CD8⁺ T cells in different anatomical location within

lung parenchyma, which is responsible for enhanced protective immunity. We did not see enhanced immunogenicity among Ag-specific CD4⁺ T_{CM} cells from metformin-treated BCG-vaccinated mice, which goes in line with no benefit of metformin-educated Ag-inexperienced CD4⁺ T cells on *Mtb* growth in adoptive transfer experiments (Fig. 1b, c). The differential effect of metformin on the CD4⁺ and CD8⁺ cells in naive or vaccinated host is not clear at present. However, as metformin normalizes CD4⁺ T-cell mitochondrial function to alleviate lupus in B6.Sle1.Sle2.Sle3 mice⁶³ and aging-associated inflammation⁶⁴ in humans, an effect of metformin on CD4⁺ T-cell metabolism in *Mtb*-infected hosts cannot be excluded. Nevertheless, our results support the concept of enhancing the efficacy of BCG vaccine by small molecule drugs⁶⁵.

In conclusion, the data presented here show that metformin shifts CD8⁺ T-cell metabolism, leading to the expansion of a memory-like CD8⁺CXCR3⁺ phenotype with functional properties that contribute to host control of *Mtb* infection and disease. Our findings are in line with evidence that metabolic reprogramming by metformin reverses CD8⁺ T-cell dysfunction during chronic *Mtb* infection⁶⁶. Our current and previously reported studies show that metformin ameliorates TB immune pathology, whereas others reported that it reverses established pulmonary fibrosis in the bleomycin model⁶⁷. That evidence, together with our demonstration that metformin enhances BCG vaccine immunogenicity and protective efficacy adds to the basis in evidence supporting metformin as a candidate for TB-HDT and as a TB vaccine adjunct.

Methods

Healthy human samples. PBMCs were isolated from eight male healthy non-obese volunteers without medication, kidney function loss, or metabolic disorders, who had received metformin for 5 days in increasing doses starting at 500 mg once a day and ending with 1000 mg twice a day⁴⁶. Blood was drawn at baseline time point before metformin intake (T0) and immediately after metformin intake on day 6 (T6).

Diabetic human patient cohort. Patients with T2D included in the study are part of the Singapore Longitudinal Aging study 2 (SLAS-2), which is a population-based cohort to study the biology of aging among Singaporean elderly individuals >55 years old⁶⁸. PBMCs from the blood samples collected from overnight fasting individuals were washed with PBS and cryopreserved in liquid nitrogen. PBMCs were thawed and used for flow cytometric staining. Fasting blood glucose, blood count, hematocrit level, albumin, creatinine, estimated glomerular filtration rate was performed on the blood samples.

Animals. CD45.1, CD45.2, *Cxcr3*^{-/-}, *Tcrβδ*^{-/-}, and OT-I mice were obtained from SiGn mouse core. All mice strains were on C57BL/6J background. CD45.1 and CD45.2 mice for chimeric in vivo experiments were obtained from Jackson Labs (Bar Harbor, USA), and performed at UMMS. For all in vivo experiments female mice aged between 8 and 12 weeks were used. Hartley strain female guinea pigs aged between 7 and 8 weeks (350–400 g) were obtained from Charles Rivers (Wilmington, MA), maintained on a normal chow diet, acclimated for 1 week then randomly assigned to four groups. Animals were housed in the SPF and BSL3 animal facilities on a 12/12 h light/dark cycle, with food and water ad libitum.

Metformin treatment for mice and guinea pigs. Metformin (1,1-Dimethylbiguanide hydrochloride, Sigma Aldrich) was provided to mice in drinking water (1.83 mg/ml which is equivalent to 270 mg/kg). Details of metformin treatment for different experimental models is provided in the figures. Guinea pigs were treated with 25 mg/kg of metformin suspended in carrier (Ora-Sweet, Paddock Laboratories, Minneapolis, MN), or carrier alone, and administered orally once daily, for 30 days, prior to *Mtb* infection. The metformin dose was determined in guinea pigs based on PK/PD analysis in which the peak plasma concentration reached 1.1 μg/mL (peak plasma concentration in human 1.1 μg/mL).

BCG vaccination. Female mice aged 8–10 weeks were vaccinated subcutaneous with a single dose BCG Pasteur strain (1 × 10⁶ colony-forming units (CFU) in 100 μl PBS). In BCG-vaccinated mice metformin treatment was initiated 1 day post vaccination. Guinea pigs were vaccinated intra-dermally (i.d) with 1 × 10⁵ BCG Pasteur strain. In vaccinated guinea pigs metformin treatment was initiated

14 days post vaccination. Sham vaccinated guinea pigs received an equal volume of saline i.d.

Mtb infection. Female mice were infected via aerosol or intra tracheal (i.t.)⁶⁹ route with *Mtb* H37Rv or *Mtb* Erdman to deliver 100–200 viable bacilli per lung. For BCG infection experiments, 10×10^6 BCG bacilli were used. The implanted bacterial loads in the lungs of infected mice were quantified 1 day post infection. Guinea pigs were infected with the *Mtb* H37Rv by aerosol to deliver 10–20 bacilli per animal and confirmed by culture.

Modified Cornell model. Starting 40 days p.i. *Mtb*-infected female mice were given INH (10 µg/mL) and PZA (15 mg/mL) in drinking water ad libitum⁷⁰ for 70 days. This was followed by a 40 day rest for all treatments. Subsequently, at day 150 p.i. mice were treated with 1 mg/mL of dexamethasone in drinking water for 15 days.

Culturing of mycobacterial strains. *Mtb* H37Rv, Erdman, and *M. bovis* BCG were grown in Middlebrook 7H9 broth (BBL Microbiology Systems) supplemented with 10% ADS (Albumin, Dextrose, Saline, Sigma) enrichment medium with 140 mM NaCl, 0.5% glycerol and 0.5% Tween-80 at 37 °C for 5–10 days to an OD₆₀₀ of 0.4–0.5. Bacterial cultures were harvested, re-suspended in 7H9 broth with 20% glycerol, and aliquots were frozen at –80 °C until later use. Before infection, cells were thawed, washed, and sonicated. Viable cell counts per mL in thawed aliquots were determined by plating serial dilutions on to Middlebrook 7H11 agar plates supplemented with 10% OADC (Oleic acid, Albumin, Dextrose, Catalase, BBL Microbiology Systems) and 0.5% glycerol followed by incubation at 37 °C for three weeks.

Enumeration of Mtb load in the tissues of infected animals. Mycobacterial loads in lung and spleen of euthanized mice were evaluated at different time points post infection by homogenizing the organs in PBS or PBS with 0.05% Tween-80 using MACS tissue dissociator (Miltenyi Biotec). Guinea pigs were killed with an intra-peritoneal overdose of pentobarbital (>120 mg/kg), and representative lung tissue samples were collected sterilely and homogenized in 9 ml of sterile saline. Tenfold serial dilutions of tissue homogenates in sterile PBS were plated in triplicates on Middlebrook 7H11 agar plates supplemented with 10% OADC and 0.5% glycerol, incubated for 3–6 weeks at 37 °C and CFUs counted.

Cell isolation from lungs and spleens. Lungs were aseptically isolated from mice and incubated at 37 °C in 10% FBS RPMI media containing 1.4 mg/ml collagenase A (Roche) and 30 µg/ml DNase I for 60 min. The treated lung tissue and spleen was dissociated over the 70 µm cell strainer (Fisherbrand). Strainer was washed to collect single-cell suspension. Red blood cells were lysed with ACK lysing buffer (Lonza) for 5 min following by washing of cells with culture media. Cells were counted and adjusted to 5×10^6 cells/ml.

Magnetic sorting of murine T cells. Spleen cells were washed twice in fresh magnetic-activated cell sorting (MACS) buffer. CD4⁺ and CD8⁺ T cells were magnetically purified via negative selection using Dynabeads or MACS cell separation system (Supplementary Table 7) according to the manufacturer's protocols, followed by purity check which was around 90–95%.

FACS sorting of murine memory CD8⁺ T cells. MACS-sorted splenic CD8⁺ T cells were stained with live dead marker, blocked with Fc block and surface stained with anti-CD3-FITC, anti-CD4-Pacific blue, anti-CD8-APC-Cy7, anti-CD44-BV650, and anti-CD62L-PE-Cy7 (Supplementary Table 8). Stained cells were sorted on fluorescence-activated cell sorting (FACS) Aria II, FACS Aria III, or BD Influx (Becton Dickinson, San Jose, CA, USA), followed by purity check which was ~90–95%.

Adoptive T-cell transfers. Purified splenic CD4⁺ or CD8⁺ T cells from untreated or metformin-treated CD45.1 WT or CD45.2 WT mice were transferred via tail vein injection into sub lethally irradiated (600 rads) CD45.2 WT mice (Fig. 1). MACS-sorted splenic CD8⁺ T cells or T_M or T_E from untreated or metformin-treated CD45.1 WT mice were transferred via intra orbital injection into CD45.2 WT or *Tcrβ8*^{-/-} (Fig. 3d, e). The details of number of T cells transferred are in Supplementary Table 9.

Metabolism assays. Real-time mitochondrial OCR and ECAR of splenic CD8⁺ T cells was measured in media (Dulbecco's modified eagle medium; DMEM containing 25 mM glucose and 2 mM L-glutamine), in response to 1 µM oligomycin, 5 µM FCCP, and 0.5 µM rotenone/antimycin A, using Seahorse XF Cell Mito Stress and Glyco Stress Test Kit and XFe96 Extracellular Flux Analyzer (Agilent Technologies, USA, Supplementary Table 7). FAO assay were carried out using Seahorse XF Palmitate-BSA FAO Substrate kit in media (KHB containing 2.5 mM glucose and 0.5 mM Carnitine) in response to 1 µM oligomycin, 1 µM FCCP, and 0.5 µM rotenone/antimycin A. For FAO assay, cells were prior starved in Seahorse DMEM medium (DMEM containing 0.5 mM glucose, 1 mM L-glutamine, and 0.5 mM

Carnitine) for 2 hrs. Also for FAO assay, BSA or Palmitate:BSA was added into the 96-well plate and 200 µM etomoxir were used additionally as drug injection. SRC was determined as the absolute increase in OCR after FCCP injection compared with basal OCR. Data was analyzed with Wave software, version 2.4 (Agilent Technologies).

Flow cytometry. Single-cell suspensions of spleens, lungs, and lymph nodes (from mice) were prepared at the indicated time points. Live dead staining was performed for 15 minutes at room temperature or for 20 minutes at 37 °C. Non-specific antibody binding was blocked by adding anti-CD16/32 (Fc block) (BD Biosciences). Following this surface markers were stained for 20–25 minutes at 4 °C with the following anti-mouse antibodies: anti-CD45-Pacific blue/BV605/ FITC, CD45.1-BV711, CD45.2-APC, anti-CD3-FITC/ Pacific blue/ BUV395/ PerCP-Cy5.5, anti-CD4-Pacific blue/Alexa Fluor 700/PerCP-Cy5.5/PE, anti-CD8-APC-Cy7/ FITC, anti-CD44-BV650/ PE-Cy7/ PE-Cy5, anti-CD62L- PE-Cy7/ PE-CF594 and anti-CXCR3-BV605 (Supplementary Table 8). In some experiments, mitochondrial staining was performed with 200 nM Mitotracker green and/or 20 µM TMRM in RPMI media without FCS for 30 minutes at 37 °C prior to staining of surface markers.

For intracellular cytokine staining, spleen cells were ex vivo stimulated for 20 h with 40 µg/ml PPD (purified protein derivative, Statens Serum Institute, Denmark) in the presence of Golgi StopTM (BD Biosciences) and Monensin (1000×, BioLegend) for the last 4 hours, at 37 °C and 5% CO₂. In some experiment's spleen cells were ex vivo stimulated with IL-2 and TB10.4 peptides for 5 hours at 37 °C. Brefeldin A was added to the stimulation for the last 4 hours. Live dead staining and blocking was performed. Cells were then stained with anti-CD45-BV605, anti-CD3-Pacific blue/PerCP-Cy5.5, anti-CD4-PE/Alexa Fluor 700, anti-CD8a-APC-Cy7/FITC, anti-CD44-PE-Cy7/PE-Cy5 and anti-CD62L-AlexaFluor 700/PE-Cy7 antibodies for 25 min at 4 °C (Supplementary Table 8). After washing, cells were fixed and permeabilized for 20 minutes with Cytotfix/CytopermTM (BD Biosciences). Permeabilized cells were washed with Perm/Wash bufferTM (BD Biosciences) and stained with anti-IFN-γ-APC/BV 421, TNF-APC or Perforin-PE antibody for 25 minutes at 4 °C. Subsequently, cells were fixed in 2% paraformaldehyde before acquisition.

Human PBMCs were stained with live dead marker and following anti-human antibodies: anti-CD34-PE, anti-CD4-BV750, anti-CD8-BV605, anti-CD14-BV605, anti-TCRγ/δ-APCR700, anti-CD27-BV510, anti-CD45-BUV805, anti-CxCR3-BV650, anti-TCRVδ2-BV711, anti-CD3-BV570, anti-Va7.2-APC-Cy7, anti-CD45RO-PerCP/Cy5.5, and anti-CD161-BV785 (Supplementary Table 10). Dilution of different antibodies used was either 1:50, 1:100, or 1:200. Each antibody was validated for flow cytometry staining as per manufacturer's description. Fluorescence-minus-one and isotype controls were used during validation. Stained cells were acquired using a LSRII cytometer with five lasers (BD, San Jose, CA, USA) or Fortessa cytometer with four lasers (Becton Dickinson, San Jose, CA, USA) or Symphony cytometer (BD Biosciences, California, USA) and data was collected using FACSDivaTM version 7 (BD Biosciences). Flow cytometry data were analyzed with FlowJoTM version 10.3 (Tree Star, Inc., USA).

Assessment of caspase-1 activity. The activity of caspase-1 was determined using fluorescent inhibitor of caspase-1 (FAM-Flica Caspase-1 Assay kit, ImmunoChemistry Technologies). Staining procedure was performed according to manufactures protocol. In brief after live/dead and surface antibody staining of lung and spleen single cells, FLICA reagent FAM-YVAD-FMK was provided to single cells and binding to activated caspase-1 was allowed for 1 h at 37 °C in the dark. Stained cells were washed with apoptosis wash buffer, followed by fixation. The green fluorescent was detected in FITC channel and samples were acquired using LSRII cytometer.

Glucose uptake assay. 2-(N-(7-nitrobenz-2-oxa-1,3-diazol-4-yl)amino)-2-deoxyglucose (2-NBDG) uptake was performed on glucose-deprived cultures of spleen and lung single cells. Cells were incubated in media containing 200 µM 2-NBDG for 20 minutes at 37 °C. Followed this live dead and surface marker staining was performed. Fluorescent of 2-NBDG was detected in FITC channel using Fortessa cytometer.

CyTOF staining and data analysis. Spleen and lung cells from mice, and human PBMCs were first stained with 200 µM cisplatin (Sigma) for the discrimination of dead cells. Upon this, cells were washed and stained with a primary antibodies cocktail for 30 minutes at 4 °C (Supplementary Table 1 (for human antibodies) and Supplementary Table 5 (for mouse antibodies)). Dilution of different antibodies used was either 1:100 or 1:200 and was standardized by our CyTOF platform. After washing, cells were stained with the heavy metal-labeled antibodies cocktail for 30 minutes at 4 °C. Cells were washed, fixed and permeabilized using fixation FoxP3 buffer (eBioscience) for 45 minutes at 4 °C. Upon this cells were stained with intranuclear antibodies cocktail for 30 minutes at 4 °C. Labeled cells were washed twice with PBS and fixed in 2% or 4% PFA overnight. Subsequently, cells were washed and stained for barcodes (30 minutes at 4 °C) and DNA (10 minutes at 4 °C). Samples were acquired on the Helios CyTOF (Fluidigm), and analyzed as mentioned before^{24,25,71}. For details, see supplementary methods.

Ex vivo culture of primary T cells. OT-1 splenocytes were activated with 20 µg/ml OVA protein (Invivogen) and 100 U/ml hIL-2 (Miltenyi Biotec) and cultured in IMDM media (supplemented with 10% FBS, 2 mM L-glutamine, 1 mM Sodium pyruvate, 0.1 mM NEAA, 1% Kanamycin) for 3 days. After washing, cells were subsequently cultured with 0.4, 2, 10 ng/ml of hIL-15 (R&D) and/or 2 mM MET for 4 days. IL-15-derived antigen-specific CD8⁺ T cells were analyzed for memory markers by flow cytometry.

Real-time quantitative RT-PCR. Cells or tissues were lysed in TRIzol Reagent (Invitrogen), and total RNA was extracted using the RNeasy Mini Kit (Qiagen). RNA was reverse-transcribed using the iScript cDNA synthesis Kit (Bio-Rad). Complementary DNA (cDNA) was used for real-time quantitative PCR using 2x iQ SYBR Green supermix and C1000 Thermal Cycler (Bio-Rad) using specific primers (see supplemental methods). The relative mRNA expression level of each gene was normalized to *Gapdh* housekeeping gene expression in the untreated condition, and fold induction was calculated by the $\Delta\Delta CT$ method relative to those in untreated cells per tissue.

RNAseq and analysis. Total RNA was extracted following the double extraction protocol: RNA isolation by TRIzol followed by a Qiagen RNeasy Micro clean-up procedure (Qiagen, Hilden, Germany). The extracted RNA samples were inspected on Agilent Bioanalyzer (Agilent Technologies, Santa Clara, CA) for quality assessment. All RNA samples were analyzed on Perkin Elmer Labchip GX system (Perkin Elmer, Waltham, MA, USA) for quality assessment with a median RNA Quality Score of 9. cDNA libraries were prepared using 500 pg of total RNA and 1 µl of a 1:200,000 dilution of ERCC RNA Spike in Controls (Ambion, Thermo Fisher Scientific, Waltham, MA, USA) using SMARTSeq v2 protocol⁷² except for the following modifications: 1. Use of 20 µM TSO; 2. Use of 250 pg of cDNA with 1/5 reaction of Illumina Nextera XT kit (Illumina, San Diego, CA, USA). The length distribution of the cDNA libraries was monitored using DNA High Sensitivity Reagent Kit on the Perkin Elmer Labchip GX system (PerkinElmer, Waltham, MA, USA). The libraries were qPCR quantified (Kapa Biosystems, Wilmington, MA) to ascertain the loading concentration. RNAseq libraries of FACS sorted CD8 T_M cells subjected to an indexed PE sequencing run of 2 × 51 cycles on an Illumina HiSeq 2000. FASTQ files were checked for quality control issues using fastQC and none were found. The reads in the FASTQ files were mapped onto the mouse genome build mm10 using STAR and the gene counts counted using featureCounts (part of the Subread package). DEGs were detected using DESeq2⁷³ running in R version 3.3.3. DEGs having a *p* value <0.05 (calculated by DESeq2⁷³ using *t* test) were considered to be statistically significant. DEGs were used in IPA for a core analysis. IPA uses Fisher's exact test to determine the probability of the association of genes with the pathway/molecular function. Heat maps were generated using the package ComplexHeatmap in R version 3.3.3.

Enrichment of FOXO1 targets. The overlap between the DEGs from the RNAseq comparison of CD8⁺ T cells from *Cxcr3*^{-/-} vs WT mice and the FOXO1 target genes from Webb et al.³⁶ was determined (Supplementary Data 1). The hypergeometric distribution was used to determine the significance of this overlap/enrichment using all the RNAseq genes tested and the genes analyzed in Webb et al.³⁶ as the background. A *p* value of <0.05 was considered to be significant. Analysis conducted in R version 3.3.3.

Histology and morphometry of guinea pigs lung samples. Left caudal lung lobe of guinea pigs was collected for histopathology and was fixed in 4% paraformaldehyde for >48 hours, processed and embedded in paraffin, sectioned and stained with hematoxylin and eosin. The *Mtb* lesion burden was determined morphometrically using the area fraction fractionator method with Stereo investigator software (MBF Biosciences, Williston, VT). The data was expressed as the percent of lung area affected by characteristic *Mtb* lesions. Photomicrographs were obtained from tissue sections representative of the mean values within individual animal treatment groups.

Statistical analysis. All values are mean ± SD or SEM of individual samples. Data analysis was performed with GraphPad Prism Software (GraphPad Software Inc., version 7.01). The statistical tests utilized are two-tailed and respective details have been indicated in figure legends.

Study approval. The study was approved by the Institutional Biosafety Committee (IBC) and Institutional Animal Care and Use Committee (IACUC) of the (i) Biological Resource Council (BRC), A*STAR, Singapore; (ii) Defence Science Organization (DSO) national laboratories, Singapore, (iii) Colorado State University, USA, and (iv) University of Massachusetts Medical School (UMMS), USA. The study in human healthy volunteers and diabetic patients was approved by the Arnhem-Nijmegen Ethical Committee (NL47793.091.14) and National University of Singapore Institutional Review Board (NUS-IRB #04-140), respectively. Informed consent from all participants was obtained.

Reporting summary. Further information on research design is available in the Nature Research Reporting Summary linked to this article.

Data availability

RNAseq data that support the findings of this study have been deposited in GeneBank GEO, accession [GSE139948](https://www.ncbi.nlm.nih.gov/geo/query/acc.cgi?acc=GSE139948). Other data are available from the corresponding author upon request.

Received: 6 January 2020; Accepted: 28 September 2020;

Published online: 16 October 2020

References

- Wallis, R. S. & Hafner, R. Advancing host-directed therapy for tuberculosis. *Nat. Rev. Immunol.* **15**, 255–263 (2015).
- Kaufmann, S. H. E., Dorhoi, A., Hotchkiss, R. S. & Bartenschlager, R. Host-directed therapies for bacterial and viral infections. *Nat. Rev. Drug Disco.* **17**, 35–56 (2018).
- Singhal, A. et al. Metformin as adjunct antituberculosis therapy. *Sci. Transl. Med.* **6**, 263ra159 (2014).
- Magee, M. J., Salindri, A. D., Kornfeld, H. & Singhal, A. Reduced prevalence of latent tuberculosis infection in diabetes patients using metformin and statins. *Eur. Respir. J.* **53**, 1801695 (2019).
- Pan, S. W. et al. The risk of TB in patients with type 2 diabetes initiating metformin vs sulfonylurea treatment. *Chest* **153**, 1347–1357 (2018).
- Lin, S. Y. et al. Metformin is associated with a lower risk of active tuberculosis in patients with type 2 diabetes. *Respirology* **23**, 1063–1073 (2018).
- Tseng, C. H. Metformin decreases risk of tuberculosis infection in type 2 diabetes patients. *J. Clin. Med.* **7**, 264 (2018).
- Degner, N. R., Wang, J. Y., Golub, J. E. & Karakousis, P. C. Metformin use reverses the increased mortality associated with diabetes mellitus during tuberculosis treatment. *Clin. Infect. Dis.* **66**, 198–205 (2018).
- Lee, Y. J. et al. The effect of metformin on culture conversion in tuberculosis patients with diabetes mellitus. *Korean J. Intern. Med.* **33**, 933–940 (2018).
- Lin, P. L. & Flynn, J. L. CD8 T cells and Mycobacterium tuberculosis infection. *Semin. Immunopathol.* **37**, 239–249 (2015).
- Graef, P. et al. Serial transfer of single-cell-derived immunocompetence reveals stemness of CD8(+) central memory T cells. *Immunity* **41**, 116–126 (2014).
- Haluszcak, C. et al. The antigen-specific CD8⁺ T cell repertoire in unimmunized mice includes memory phenotype cells bearing markers of homeostatic expansion. *J. Exp. Med.* **206**, 435–448 (2009).
- Lee, Y. J., Jameson, S. C. & Hogquist, K. A. Alternative memory in the CD8 T cell lineage. *Trends Immunol.* **32**, 50–56 (2011).
- Huang, W., Hu, J. & August, A. Cutting edge: innate memory CD8⁺ T cells are distinct from homeostatic expanded CD8⁺ T cells and rapidly respond to primary antigenic stimuli. *J. Immunol.* **190**, 2490–2494 (2013).
- Lee, J. Y., Hamilton, S. E., Akue, A. D., Hogquist, K. A. & Jameson, S. C. Virtual memory CD8 T cells display unique functional properties. *Proc. Natl Acad. Sci. USA* **110**, 13498–13503 (2013).
- Lin, J. S. et al. Virtual memory CD8 T cells expanded by helminth infection confer broad protection against bacterial infection. *Mucosal Immunol.* **12**, 258–264 (2019).
- Lauvau, G., Boutet, M., Williams, T. M., Chin, S. S. & Chorro, L. Memory CD8 (+) T cells: innate-like sensors and orchestrators of protection. *Trends Immunol.* **37**, 375–385 (2016).
- Geltink, R. I. K., Kyle, R. L. & Pearce, E. L. Unraveling the complex interplay between T cell metabolism and function. *Annu. Rev. Immunol.* **36**, 461–488 (2018).
- Krauss, S., Brand, M. D. & Buttgerit, F. Signaling takes a breath—new quantitative perspectives on bioenergetics and signal transduction. *Immunity* **15**, 497–502 (2001).
- van der Windt, G. J. et al. Mitochondrial respiratory capacity is a critical regulator of CD8⁺ T cell memory development. *Immunity* **36**, 68–78 (2012).
- Pearce, E. L. et al. Enhancing CD8 T-cell memory by modulating fatty acid metabolism. *Nature* **460**, 103–107 (2009).
- Quinn, K. M. et al. Metabolic characteristics of CD8(+) T cell subsets in young and aged individuals are not predictive of functionality. *Nat. Commun.* **11**, 2857 (2020).
- Gallegos, A. M. et al. A gamma interferon independent mechanism of CD4 T cell mediated control of *M. tuberculosis* infection in vivo. *PLoS Pathog.* **7**, e1002052 (2011).
- Cheng, C. Y. et al. Host sirtuin 1 regulates mycobacterial immunopathogenesis and represents a therapeutic target against tuberculosis. *Sci. Immunol.* **2**, eaaj1789 (2017).

25. Fehlings, M. et al. Checkpoint blockade immunotherapy reshapes the high-dimensional phenotypic heterogeneity of murine intratumoural neoantigen-specific CD8(+) T cells. *Nat. Commun.* **8**, 562 (2017).
26. Groom, J. R. & Luster, A. D. CXCR3 in T cell function. *Exp. Cell Res.* **317**, 620–631 (2011).
27. Koch, M. A. et al. The transcription factor T-bet controls regulatory T cell homeostasis and function during type 1 inflammation. *Nat. Immunol.* **10**, 595–602 (2009).
28. Hu, J. K., Kagari, T., Clingan, J. M. & Matloubian, M. Expression of chemokine receptor CXCR3 on T cells affects the balance between effector and memory CD8 T-cell generation. *Proc. Natl Acad. Sci. USA* **108**, E118–E127 (2011).
29. Slutter, B., Pewe, L. L., Kaech, S. M. & Harty, J. T. Lung airway-surveillance CXCR3(hi) memory CD8(+) T cells are critical for protection against influenza A virus. *Immunity* **39**, 939–948 (2013).
30. Schluns, K. S., Williams, K., Ma, A., Zheng, X. X. & LeFrancis, L. Cutting edge: requirement for IL-15 in the generation of primary and memory antigen-specific CD8 T cells. *J. Immunol.* **168**, 4827–4831 (2002).
31. Kurachi, M. et al. Chemokine receptor CXCR3 facilitates CD8(+) T cell differentiation into short-lived effector cells leading to memory degeneration. *J. Exp. Med.* **208**, 1605–1620 (2011).
32. Kimura, M. Y. et al. IL-7 signaling must be intermittent, not continuous, during CD8(+) T cell homeostasis to promote cell survival instead of cell death. *Nat. Immunol.* **14**, 143–151 (2013).
33. Gattinoni, L. et al. Wnt signaling arrests effector T cell differentiation and generates CD8+ memory stem cells. *Nat. Med.* **15**, 808–813 (2009).
34. Haque, M. et al. C-Myc regulation by costimulatory signals modulates the generation of CD8+ memory T cells during viral infection. *Open Biol.* **6**, 150208 (2016).
35. Delpoux, A. et al. Continuous activity of Foxo1 is required to prevent anergy and maintain the memory state of CD8(+) T cells. *J. Exp. Med.* **215**, 575–594 (2018).
36. Webb, A. E., Kundaje, A. & Brunet, A. Characterization of the direct targets of FOXO transcription factors throughout evolution. *Aging Cell* **15**, 673–685 (2016).
37. Kim, M. V., Ouyang, W., Liao, W., Zhang, M. Q. & Li, M. O. The transcription factor Foxo1 controls central-memory CD8+ T cell responses to infection. *Immunity* **39**, 286–297 (2013).
38. Link, W. & Fernandez-Marcos, P. J. FOXO transcription factors at the interface of metabolism and cancer. *Int. J. Cancer* **141**, 2379–2391 (2017).
39. Cabrera-Ortega, A. A., Feinberg, D., Liang, Y., Rossa, C. Jr. & Graves, D. T. The role of forkhead box 1 (FOXO1) in the immune system: dendritic cells, T cells, B cells, and hematopoietic stem cells. *Crit. Rev. Immunol.* **37**, 1–13 (2017).
40. Wilhelm, K. et al. FOXO1 couples metabolic activity and growth state in the vascular endothelium. *Nature* **529**, 216–220 (2016).
41. Raud, B. et al. Etomoxir actions on regulatory and memory T cells are independent of Cpt1a-mediated fatty acid oxidation. *Cell Metab.* **28**, 504–515 e507 (2018).
42. Nair, V. et al. Mechanism of metformin-dependent inhibition of mammalian target of rapamycin (mTOR) and Ras activity in pancreatic cancer: role of specificity protein (Sp) transcription factors. *J. Biol. Chem.* **289**, 27692–27701 (2014).
43. John, G. B. et al. The mitochondrial inner membrane protein mitofilin controls cristae morphology. *Mol. Biol. Cell* **16**, 1543–1554 (2005).
44. Man, S. M. & Kanneganti, T. D. Converging roles of caspases in inflammasome activation, cell death and innate immunity. *Nat. Rev. Immunol.* **16**, 7–21 (2016).
45. Ordway, D. et al. The cellular immune response to Mycobacterium tuberculosis infection in the guinea pig. *J. Immunol.* **179**, 2532–2541 (2007).
46. Lachmandas, E. et al. Metformin alters human host responses to Mycobacterium tuberculosis in healthy subjects. *J. Infect. Dis.* **220**, 139–150 (2019).
47. Romero, P. et al. Four functionally distinct populations of human effector-memory CD8+ T lymphocytes. *J. Immunol.* **178**, 4112–4119 (2007).
48. Grayson, J. M., Zajac, A. J., Altman, J. D. & Ahmed, R. Cutting edge: increased expression of Bcl-2 in antigen-specific memory CD8+ T cells. *J. Immunol.* **164**, 3950–3954 (2000).
49. Foreman, T. W. et al. CD4+ T-cell-independent mechanisms suppress reactivation of latent tuberculosis in a macaque model of HIV coinfection. *Proc. Natl Acad. Sci. USA* **113**, E5636–E5644 (2016).
50. Scanga, C. A. et al. Reactivation of latent tuberculosis: variations on the Cornell murine model. *Infect. Immun.* **67**, 4531–4538 (1999).
51. Young, C., Walzl, G. & Du Plessis, N. Therapeutic host-directed strategies to improve outcome in tuberculosis. *Mucosal Immunol.* **13**, 190–204 (2019).
52. White, J. T., Cross, E. W. & Kedl, R. M. Antigen-inexperienced memory CD8(+) T cells: where they come from and why we need them. *Nat. Rev. Immunol.* **17**, 391–400 (2017).
53. Alanio, C. et al. CXCR3/CXCL10 axis shapes tissue distribution of memory phenotype CD8(+) T cells in nonimmunized mice. *J. Immunol.* **200**, 139–146 (2018).
54. Oghumu, S. et al. Distinct populations of innate CD8+ T cells revealed in a CXCR3 reporter mouse. *J. Immunol.* **190**, 2229–2240 (2013).
55. Oghumu, S. et al. CXCR3 expression defines a novel subset of innate CD8+ T cells that enhance immunity against bacterial infection and cancer upon stimulation with IL-15. *FASEB J.* **29**, 1019–1028 (2015).
56. van der Windt, G. J. et al. CD8 memory T cells have a bioenergetic advantage that underlies their rapid recall ability. *Proc. Natl Acad. Sci. USA* **110**, 14336–14341 (2013).
57. Rolf, J. et al. AMPKalpha1: a glucose sensor that controls CD8 T-cell memory. *Eur. J. Immunol.* **43**, 889–896 (2013).
58. Blagih, J. et al. The energy sensor AMPK regulates T cell metabolic adaptation and effector responses in vivo. *Immunity* **42**, 41–54 (2015).
59. Adams, W. C. et al. Anabolism-associated mitochondrial stasis driving lymphocyte differentiation over self-renewal. *Cell Rep.* **17**, 3142–3152 (2016).
60. Lepez, A. P. et al. Long-term homeostatic T cell proliferation is driven by AMPK-dependent regulation of oxygen reactive species. *Biorxiv* (2020) <https://doi.org/10.1101/2020.03.06.978791>.
61. Tzelepis, F. et al. Mitochondrial cyclophilin D regulates T cell metabolic responses and disease tolerance to tuberculosis. *Sci. Immunol.* **3**, eaar4135 (2018).
62. Jeyanathan, M. et al. CXCR3 signaling is required for restricted homing of parenteral tuberculosis vaccine-induced T cells to both the lung parenchyma and airway. *J. Immunol.* **199**, 2555–2569 (2017).
63. Yin, Y. et al. Normalization of CD4+ T cell metabolism reverses lupus. *Sci. Transl. Med.* **7**, 274ra218 (2015).
64. Bharath, L. P. et al. Metformin enhances autophagy and normalizes mitochondrial function to alleviate aging-associated inflammation. *Cell Metab.* **32**, 44–55 e46 (2020).
65. Bhattacharya, D. et al. Simultaneous inhibition of T helper 2 and T regulatory cell differentiation by small molecules enhances Bacillus Calmette-Guerin vaccine efficacy against tuberculosis. *J. Biol. Chem.* **289**, 33404–33411 (2014).
66. Russell, S. L. et al. Compromised metabolic reprogramming is an early indicator of CD8(+) T cell dysfunction during chronic mycobacterium tuberculosis infection. *Cell Rep.* **29**, 3564–3579 e3565 (2019).
67. Rangarajan, S. et al. Metformin reverses established lung fibrosis in a bleomycin model. *Nat. Med.* **24**, 1121–1127 (2018).
68. Tizazu, A. M. et al. Metformin monotherapy downregulates diabetes-associated inflammatory status and impacts on mortality. *Front Physiol.* **10**, 572 (2019).
69. Singhal, A. et al. Experimental tuberculosis in the Wistar rat: a model for protective immunity and control of infection. *PLoS ONE* **6**, e18632 (2011).
70. Cheigh, C. I. et al. Posttreatment reactivation of tuberculosis in mice caused by Mycobacterium tuberculosis disrupted in mce1R. *J. Infect. Dis.* **202**, 752–759 (2010).
71. Levine, J. H. et al. Data-driven phenotypic dissection of aml reveals progenitor-like cells that correlate with prognosis. *Cell* **162**, 184–197 (2015).
72. Picelli, S. et al. Full-length RNA-seq from single cells using Smart-seq2. *Nat. Protoc.* **9**, 171–181 (2014).
73. Love, M. I., Huber, W. & Anders, S. Moderated estimation of fold change and dispersion for RNA-seq data with DESeq2. *Genome Biol.* **15**, 550 (2014).

Acknowledgements

We thank S1gN Flow Facility, ABSL3, BRC laboratory personnel and Yannick Simoni, Nicholas Ang, and Kandhadayar G. Srinivasan for assistance. This research was supported by S1gN A*STAR Immunomonitoring platform grant to S1gN (#BMRC/IAF/311006, #H16/99/b0/011, and #NRF2017_SISFP09); NIH Grant #R01HL081149 and #U19AI11224 (to H.K.) and #R01HL152078 (to H.K. and A.S.), ERC Advanced Grant (#833247) and a Spinoza grant of the Netherlands Organization for Scientific Research to M.G.N.

Author contributions

A.S. conceived the idea, designed the study. J.B. performed the experiments and analyzed the data. A.L. and M.M. performed the experiments. N.M.G. and H.K. performed mice adoptive transfer and BCG vaccination experiments, and analyzed the data. S.L. and E.N. analyzed CyTOF data. D.A., J.H.F., A.T., and R.B. performed Guinea pig experiments. J.L. and F.S. performed RNAseq studies and B.L. analyzed RNAseq data. E.L., T.P.N., A.M.T., A.L., M.G.N., and R.C. provided the clinical samples and related information. A.S. oversaw the study and wrote the manuscript. All authors discussed results and commented on the manuscript.

Competing interests

The authors declare no competing interests.

Additional information

Supplementary information is available for this paper at <https://doi.org/10.1038/s41467-020-19095-z>.

Correspondence and requests for materials should be addressed to A.S.

Peer review information *Nature Communications* thanks Maziar Divangahi, Thomas Lindström, and the other, anonymous reviewer(s) for their contribution to the peer review of this work.

Reprints and permission information is available at <http://www.nature.com/reprints>

Publisher's note Springer Nature remains neutral with regard to jurisdictional claims in published maps and institutional affiliations.



Open Access This article is licensed under a Creative Commons Attribution 4.0 International License, which permits use, sharing, adaptation, distribution and reproduction in any medium or format, as long as you give appropriate credit to the original author(s) and the source, provide a link to the Creative Commons license, and indicate if changes were made. The images or other third party material in this article are included in the article's Creative Commons license, unless indicated otherwise in a credit line to the material. If material is not included in the article's Creative Commons license and your intended use is not permitted by statutory regulation or exceeds the permitted use, you will need to obtain permission directly from the copyright holder. To view a copy of this license, visit <http://creativecommons.org/licenses/by/4.0/>.

© The Author(s) 2020